



KEK Preprint 91- 2
April 1991
A

20853

BEAM-BEAM PHENOMENA IN LINEAR COLLIDERS

Kaoru Yokoya

National Laboratory for High Energy Physics,
Oho, Tsukuba-shi, Ibaraki, 305, Japan

Pisin Chen

Stanford Linear Accelerator Center,
Stanford University, Stanford, CA94309, USA

ABSTRACT

The beam-beam interaction in electron-positron linear colliders shows very different aspects from that in storage rings. The single-pass nature of the linear colliders allows drastic deformation of the bunch shape during one collision. Also, under the very strong electro-magnetic field together with the high beam energy, phenomena which are not important in storage rings come into play, namely the phenomena involving the quantum field theory. The synchrotron radiation in the beam-beam field, called beamstrahlung, becomes extremely energetic. The strong field can even create electron-positron pairs from the beamstrahlung photons. In the present lecture note both the classical and quantum phenomena are described.

Lecture at 1990 US-CERN School on Particle Accelerators, Nov.7-14, 1990, Hilton Head Island, So. Carolina, USA. To be published in the school proceedings from Springer Verlag.

National Laboratory for High Energy Physics, 1991

KEK Reports are available from:

Technical Information & Library
National Laboratory for High Energy Physics
1-1 Oho, Tsukuba-shi
Ibaraki-ken, 305
JAPAN

Phone: 0298-64-1171
Telex: 3652-534 (Domestic)
(0)3652-534 (International)
Fax: 0298-64-4604
Cable: KEKOHO

BEAM-BEAM PHENOMENA IN LINEAR COLLIDERS¹

Kaoru Yokoya and Pisin Chen[†]

National Laboratory for High Energy Physics, Oho, Tsukuba-shi, Ibaraki, 305, Japan

[†]Stanford Linear Accelerator Center, Stanford University, Stanford, CA94309, USA.

1 Introduction

A linear collider is a huge complex consisting of several components each of which calls for new technologies and theoretical understandings. Among them, the problem of the beam-beam interaction seems to be the 'cleanest' one in the sense that it contains only a few numbers of parameters such as the beam size and the number of particles in a bunch and that it involves almost no technological developments.

Although the basic physics of the beam-beam interaction in linear colliders is the same as that in circular colliders, the actual theory is totally different because of the very strong interaction within one collision and the single-pass nature. The phenomena consists of two aspects, namely the classical and the quantum mechanical one. During the collision the bunches are deformed due to the electromagnetic attraction between electron and positron beams, giving rise to an enhancement of the luminosity. Because of the high energy and high beam-beam field we expect large amount of energy deposite in the form of the synchrotron radiation, which, in the case of beam-beam interaction, is called beamstrahlung. Also, since a couple of years ago, it has been recognized that the e^+e^- pair creation process is a significant source of backgrounds for the experiments.

The change of the particle energy and population due to the quantum processes can affect the classical phenomena in principle. Nevertheless, one normally chooses the design parameters such that the energy loss by beamstrahlung is only a small fraction of the initial energy and that the pair-created particles are much fewer in number than the incident particles. Therefore, to a good approximation we can discuss the classical and quantum phenomena separately. If necessary, one can take into account the effects such as the beam deformation on the quantum processes by using effective beam size.

In this report we shall mostly discuss linear colliders of the next generation in which the beam energy is upto about 1TeV.

2 Classical Phenomena

The major issues of the classical effects are the enhancement of the luminosity due to the electromagnetic attraction and the deflection angles of the individual particles and the

¹Lecture at 1990 US-CERN School on Particle Accelerators, Nov.7-14, 1990, Hilton Head Island, So. Carolina, USA

bunch center. These issues have already been studied in details by many authors[1,2,3,4,5], although there are still many topics to be studied such as asymmetric collisions. We shall describe the results so far obtained with an emphasis on symmetric collisions of flat beams, which have been commonly invoked for the purpose of suppressing the beamstrahlung.

The fact that the beam energy is much higher than the electron rest mass simplifies the problem of classical particle dynamics greatly;

- (1) The acceleration by the longitudinal field is negligible.
- (2) The transverse force between e^+ and e^- acts only when their longitudinal coordinates nearly coincide because of the Lorentz contraction.
- (3) The interaction within the same bunch can be ignored because $\mathbf{E} + \mathbf{v} \times \mathbf{B} = \mathcal{O}(\mathbf{E}/\gamma^2)$.
- (4) Only the electro-static field is needed: $\mathbf{E} + \mathbf{v} \times \mathbf{B} \sim 2\mathbf{E}$, even in the presence of a (reasonable) crossing angle.

Coordinate system

We define the coordinate (x, y, s, t) for a head-on collision such that the longitudinal coordinate s is along the direction of motion of the electron beam and that $s=t=0$ at the moment when the two bunch centroids overlap. We also define comoving longitudinal coordinate z_1 (z_2) whose origin is the center of the electron (positron) bunch. (Therefore, the coordinate (x, y, z_2, t) is left-handed.) Since particles travel almost at the speed of light, z_1 (z_2) is a constant for each particle. The s coordinate of a particle in electron (positron) bunch satisfies the relation $s = z_1 + t$ ($s = -z_2 - t$). Unless specified otherwise, we use the convention $c=\hbar=1$ throughout the discussions.

2.1 Equation of Motion and the Disruption Parameters

The equation of motion of an electron is given by

$$\frac{d^2x}{dt^2} + \frac{4Nr_e}{\gamma} n_L(z_2) \frac{\partial \Phi}{\partial x} = 0, \quad (z_2 = -z_1 - 2t). \quad (2.1)$$

(similarly for y) Here, N is the number of particles in a bunch, r_e the classical electron radius, γ the particle energy in units of rest mass and n_L the longitudinal density, which is independent of t , defined by

$$n_L(z) = \int n(x, y, z, t) dx dy \quad (2.2)$$

where the density n is normalized such that $\int n dx dy dz = 1$. The electro-static potential Φ satisfies the Poisson equation

$$\Delta \Phi \equiv \frac{\partial^2 \Phi}{\partial x^2} + \frac{\partial^2 \Phi}{\partial y^2} = 2\pi n_T(x, y, z_2, t) \quad (2.3)$$

where n_T is the transverse distribution defined by $n(x, y, z, t)/n_L(z)$.

A formal solution to the Poisson equation is given by

$$\Phi(x, y) = \frac{1}{2} \int \log[(x - X)^2 + (y - Y)^2] n_T(X, Y) dX dY. \quad (2.4)$$

If the transverse particle distribution is axisymmetric (i.e., "round" beam) and Gaussian with r. m. s. radius $\sigma = \sigma_x = \sigma_y$, then Φ is given by

$$\Phi(x, y) = \int_0^r \frac{1 - e^{-r^2/2\sigma^2}}{r} dr \quad (r^2 = x^2 + y^2). \quad (2.5)$$

If the beam is very "flat", i.e., $\sigma_x \gg \sigma_y$,

$$\frac{\partial \Phi}{\partial x} = \frac{1}{\sigma_x} e^{-x^2/2\sigma_x^2} \int_0^{x/\sigma_x} e^{-\tau^2/2} d\tau \quad (2.6)$$

$$\frac{\partial \Phi}{\partial y} = \frac{1}{\sigma_x} e^{-x^2/2\sigma_x^2} \int_0^{y/\sigma_y} e^{-\tau^2/2} d\tau \quad (|y| \ll \sigma_x). \quad (2.7)$$

(These expressions do not exactly satisfy $\partial^2 \Phi / \partial x \partial y = \partial^2 \Phi / \partial y \partial x$.)

When the transverse distribution is a uniform elliptic cylinder with radii $a_x = 2\sigma_x$ and $a_y = 2\sigma_y$, Φ can be exactly expressed as

$$\Phi = \begin{cases} \frac{1}{a_x + a_y} \left(\frac{x^2}{a_x} + \frac{y^2}{a_y} \right) & \left(\frac{x^2}{a_x^2} + \frac{y^2}{a_y^2} < 1 \right) \\ \log \frac{\sqrt{a_x^2 + q} + \sqrt{a_y^2 + q}}{a_x + a_y} + \frac{x^2 / \sqrt{a_x^2 + q} + y^2 / \sqrt{a_y^2 + q}}{\sqrt{a_x^2 + q} + \sqrt{a_y^2 + q}} & \left(\frac{x^2}{a_x^2} + \frac{y^2}{a_y^2} > 1 \right) \end{cases} \quad (2.8)$$

where $q(x, y)$ is the positive solution to the equation $x^2/(a_x^2 + q) + y^2/(a_y^2 + q) = 1$.

At a distance far from the axis for any distribution, Φ can always be given by

$$\Phi = \log r + \text{const.} \quad (r \gg \sigma_x, \sigma_y). \quad (2.9)$$

Now let us define the so-called disruption parameter. Near the center of a (transversely) Gaussian beam, we have

$$\Phi = \frac{x^2}{2\sigma_x(\sigma_x + \sigma_y)} + \frac{y^2}{2\sigma_y(\sigma_x + \sigma_y)} \quad (|x| \ll \sigma_x, \quad |y| \ll \sigma_y) \quad (2.10)$$

and the equation of motion becomes

$$\frac{d^2 x}{dt^2} + \frac{4Nr_e}{\gamma} n_L(z_2) \frac{x}{\sigma_x(\sigma_x + \sigma_y)} = 0. \quad (2.11)$$

If the initial motion of a particle is paraxial ($x = x_0, \dot{x} = 0$) and if the beam-beam force is so weak that the change of x during the collision is small, the final deflection angle is given by

$$\dot{x}_{fin} = -\frac{2Nr_e}{\gamma} \frac{x_0}{\sigma_x(\sigma_x + \sigma_y)}. \quad (2.12)$$

(Note that $\int n_L(z_2) dt = \int n_L(-z_1 - 2t) dt = 1/2$.) This is equivalent to a thin focussing lens with the focal length $\sigma_x(\sigma_x + \sigma_y)\gamma/(2Nr_e)$. The disruption parameter D is defined as the ratio of the r.m.s. bunch length σ_z to the focal length. Thus,

$$D_{x(y)} \equiv \frac{2Nr_e}{\gamma} \frac{\sigma_z}{\sigma_{x(y)}(\sigma_x + \sigma_y)}. \quad (2.13)$$

We define the disruption parameter by this expression for any initial distribution although the expression for the focal length may be different for other distributions. Therefore, the expression $D = \sigma_z/(\text{focal length})$ is only approximate. Note that the horizontal-to-vertical beam size ratio is the inverse of the ratio of the disruption parameters: $R \equiv \sigma_x/\sigma_y = D_y/D_x$.

If the longitudinal distribution is uniform, the equation of motion near the axis is

$$\frac{d^2x}{dt^2} + \frac{D_x}{\sqrt{3}\sigma_z^2}x = 0 \quad (-\sqrt{3}\sigma_z/2 < t < +\sqrt{3}\sigma_z/2), \quad (2.14)$$

which gives rise to sinusoidal oscillations. The number of oscillations is given by $\sqrt{\sqrt{3}D}/2\pi$. Russian papers often invoke the parameter $n = \sqrt{D}/2\pi$ instead of D .

The disruption parameter is the most important parameter characterizing the classical effects of the beam-beam interaction in linear colliders.

2.2 Computer Simulations

Although analytic calculations are important in understanding the physics of the collision, computer simulations are indispensable for obtaining quantitative conclusions when the dynamics involved is highly nonlinear. This is especially true for strong, single-pass collisions.

In computer simulations the bunches are usually described by ensembles of macroparticles. The number of macroparticles is typically 10^3 to 10^5 . The whole process is divided into time slices. At each time step the bunches are divided into longitudinal slices and the Poisson equation is solved in each slice. The central issue of the computing technique is how to solve this equation efficiently. We can compute the beam-beam force by using the direct Coulomb force without invoking the Poisson equation. But the computing time is proportional to the number of macroparticles squared, which is extremely large when we use more than a few thousand macroparticles.

Round beams. If the problem is exactly axi-symmetric (head-on collision of round beams), the potential Φ is a function of r only and is given by

$$\frac{\partial\Phi}{\partial r} = \frac{1}{r} \left[2\pi \int_0^r n_T(r)rdr \right], \quad (2.15)$$

where the quantity in the square bracket is the total charge within radius r and can be computed easily by counting the number of macroparticles enclosed.

Very flat beams. If the beam is very flat ($\sigma_x \gg \sigma_y$), from eq.(2.4) we obtain for $|y| \ll \sigma_x$

$$\frac{\partial\Phi}{\partial x} \sim \text{p.v.} \int \frac{n_T(X)}{x-X} dX, \quad \frac{\partial\Phi}{\partial y} \sim \pi \int n_T(x,Y) \text{sgn}(y-Y) dY \quad (2.16)$$

where $n_T(x) = \int n_T(x,Y) dY$. The horizontal force is independent of y . In the limit of very flat beams, we can ignore the horizontal motion and can replace the vertical force with

$$\frac{\partial\Phi}{\partial y} \sim \pi n(x) \int n_T(Y) \text{sgn}(y-Y) dY. \quad (2.17)$$

Note, however, that the horizontal force is always the same order of magnitude as the vertical. The former can be ignored only because its effect is small compared with the horizontal dimension of the beam. Therefore, when we need the magnitude of the beam-beam force such as in the estimation of the beamstrahlung, the horizontal force cannot be ignored.

PIC: particles-in-cells. For round or very flat beams, the problem is reduced to a one-dimensional equation and the computation is very fast. In general cases where σ_x and σ_y are comparable, we need to solve real 2-d equations. For that, we use a 2-d mesh in each longitudinal slice. The particle distribution is represented by the number of macroparticles in each cell $Q_{i,j}$ and the Laplacian is approximated by a difference

$$\Delta\Phi = \frac{\Phi_{i+1,j} - 2\Phi_{i,j} + \Phi_{i-1,j}}{(\delta x)^2} + \frac{\Phi_{i,j+1} - 2\Phi_{i,j} + \Phi_{i,j-1}}{(\delta y)^2} \quad (2.18)$$

where δx and δy are the mesh sizes. The boundary condition is given at infinity by eq.(2.9), which requires an infinite mesh region. However, the potential on the outer boundary of the mesh region can be computed explicitly by using eq.(2.4):

$$\Phi_{i,j} = \frac{1}{2} \sum_{i',j'} \log[(x_i - x_{i'})^2 + (y_j - y_{j'})^2] Q_{i',j'}. \quad (2.19)$$

(To use this formula for all the grid points is too much time consuming.) The Poisson equation can then be reduced to a matrix equation $M\Phi = Q$, which can in turn be solved by the method of LU-decomposition[6]. The decomposition is time consuming (its computing time is proportional to m^6 , m being the number of mesh in x and y dimensions), but it is needed only once if we use the same value of $\delta x/\delta y$ throughout the process. In each longitudinal slice the computing time is proportional to m^3 for solving eq.(2.19) and to m^4 for the backward substitution of the LU-method.

Instead of using the LU-decomposition, we can use Fast Fourier Transformation. If we employ the 2-d Fourier transform $\tilde{\Phi}(k_x, k_y)$ and $\tilde{n}_T(k_x, k_y)$, the Poisson equation becomes $(k_x^2 + k_y^2)\tilde{\Phi} = \tilde{n}$ and is easy to solve. (In this approach special care must be taken in constructing a Fourier transformed equation, because the Fourier transformation implicitly assumes periodic distribution.) The computing time is proportional to $m^2 \log m$. This method is advantageous if m is very large.

2.3 Luminosity Enhancement

Our primary concern in the classical effects is the enhancement of the luminosity due to the Coulomb attraction between the electron and the positron beams. The luminosity per collision ($1/\text{cm}^2$) is given by

$$L = 2N^2 \int dx dy ds dt n_1(x, y, z_1, t) n_2(x, y, z_2, t) \quad (s = z_1 + t = -z_2 - t) \quad (2.20)$$

which is to be multiplied by the repetition frequency of collisions to obtain the usually cited luminosity ($1/\text{cm}^2/\text{sec}$). In the case of a head-on collision of (transverse) Gaussian beams without disruption we have

$$L_{00} = \frac{N^2}{4\pi\sigma_x\sigma_y}. \quad (2.21)$$

This needs to be modified if there is a finite crossing angle and/or finite emittance. The latter is characterized by the parameter $A_{x(y)} = \sigma_z/\beta_{x(y)}^*$ where β^* is the beta function at the collision point. The geometrical luminosity is then given by

$$L_0 = L_{00} \times \eta(\phi_c, A) \quad (2.22)$$

where ϕ_c is the full crossing angle (we assume horizontal crossing). If the beam is very flat and Gaussian, the correction factor η can be expressed using the modified Bessel function K_0 as

$$\eta = \frac{1}{\sqrt{\pi}A_y} \exp\left[-\frac{1 + c_\phi^2/4}{2A_y^2}\right] K_0\left(\frac{1 + c_\phi^2/4}{2A_y^2}\right) \quad (c_\phi = \frac{\phi_c}{\sigma_x/\sigma_z}). \quad (2.23)$$

(We shall not include the effect of initial displacement into the definition of L_0 .) The luminosity enhancement factor H_D is defined to be the effective luminosity under disruption over the geometrical one.

$$H_D = L/L_0. \quad (2.24)$$

Analytic derivation of $H_D(D)$ is very difficult. In the case of round beams with very small D , we have

$$H_D = 1 + D \frac{\sigma_x^2 \int r dr n_T^3}{\sigma_z \int r dr n_T^2} \int_{-\infty}^{\infty} d\tau \int_0^{\infty} \tau' d\tau' n_L(\tau) n_L(\tau + \tau') \quad (2.25)$$

which gives $H_D = 1 + 2D/(3\sqrt{\pi})$ for round Gaussian beams. But this does not help very much in practice when $D \gtrsim O(1)$. We need computer simulations.

In computer simulations we must be careful with the following points. First, $H_D(D)$ is not a well-defined function if the initial motion of all the particles are parallel (i.e., zero emittance). In such a case, the particles near the axis is focused to a point, causing an infinite luminosity. The nonlinearity of the force relaxes the singularity to some extent but a weak infinity still remains. In the simulations with $A=0$, of course, an infinite luminosity does not actually appear, but the result diverges logarithmically as the mesh size decreases. When the emittance is finite ($A \neq 0$) or the depth-of-focus is non-zero, the inherent divergence of the beam tends to smear out the singularity and affect the eventual luminosity. In many recent studies of the next generation linear colliders, A_y is often as big as ~ 1 .

Another point is that the problem seems to be rather singular for large D even if $A \neq 0$. We normally expect that H_D increases with D upto a certain point and then saturates before it starts to decrease. However, it increases monotonically in some of the simulation results[3,4] which assume either exact axial symmetry for round beams or exact up-down ($+y$ and $-y$) symmetry for flat beams. This problem is still controversial but seems to be only of academic interest because the actual beams are more or less asymmetric in any case. To avoid this problem, we introduce an initial beam offset (displacement of the whole bunch) Δ . Thus, H_D is a function of D , A and Δ .

Fig.1 shows H_D for round Gaussian beams as a function of D with various values of Δ for $A = 0.4$. The curve for $\Delta=0$ (solid line) was computed assuming exact axial symmetry.

Fig.1. Luminosity enhancement factor for round Gaussian beams for various values of the offset. $A=0.4$.

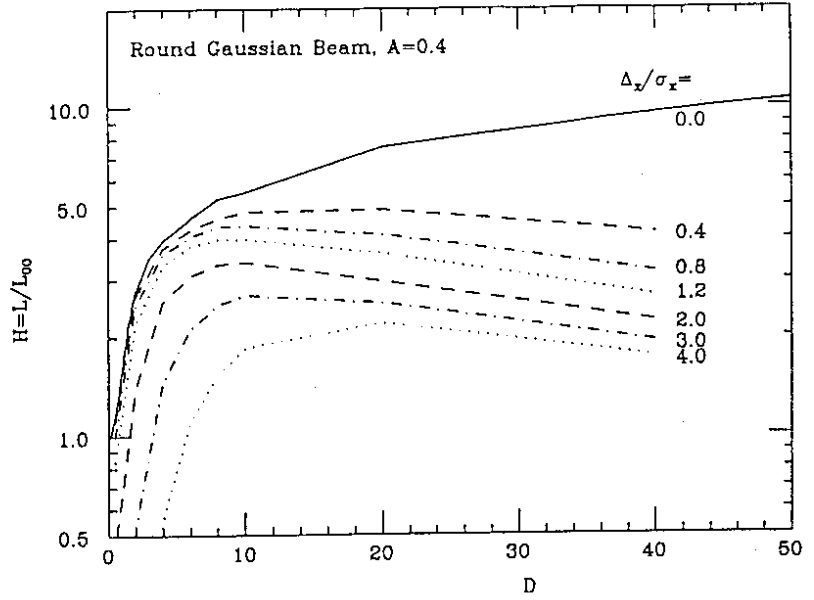
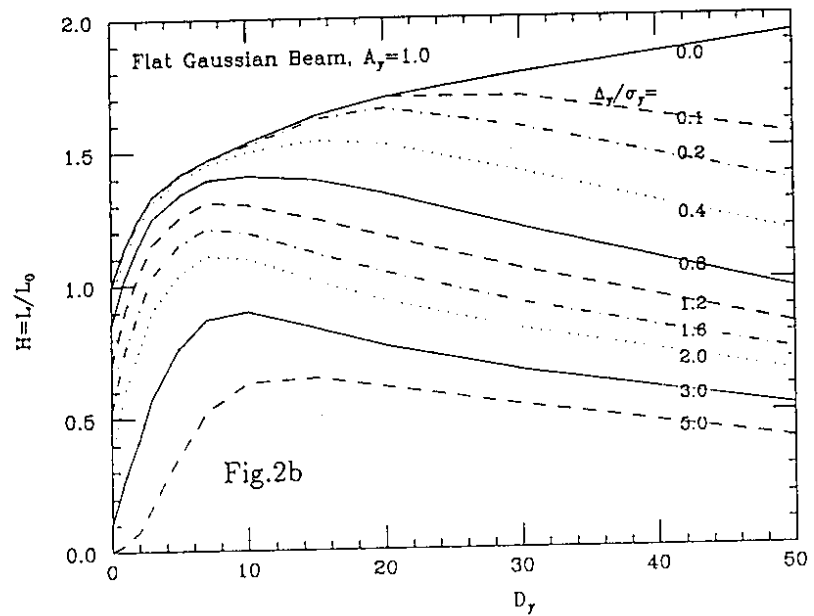
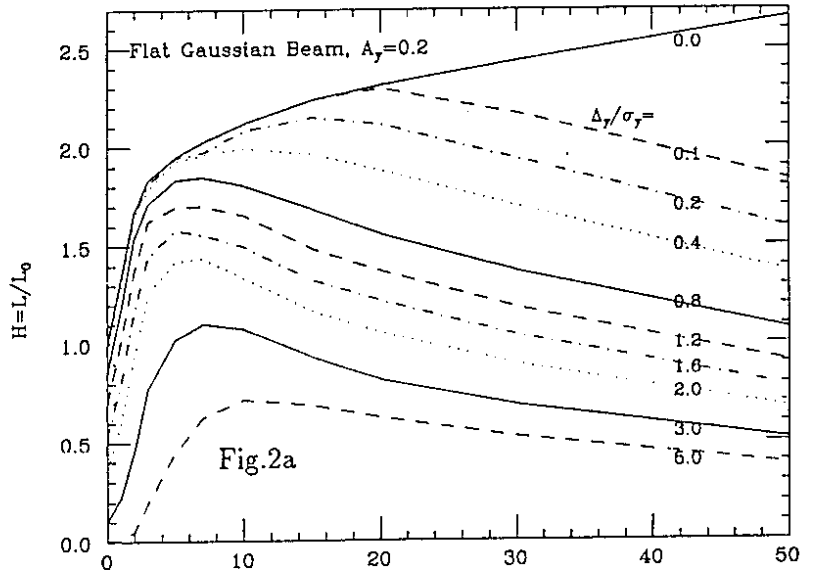


Fig.2. Enhancement factor for flat Gaussian beams for various values of the offset Δ_y . $A_y=0.2$ in Fig.2a and 1.0 in Fig.2b.



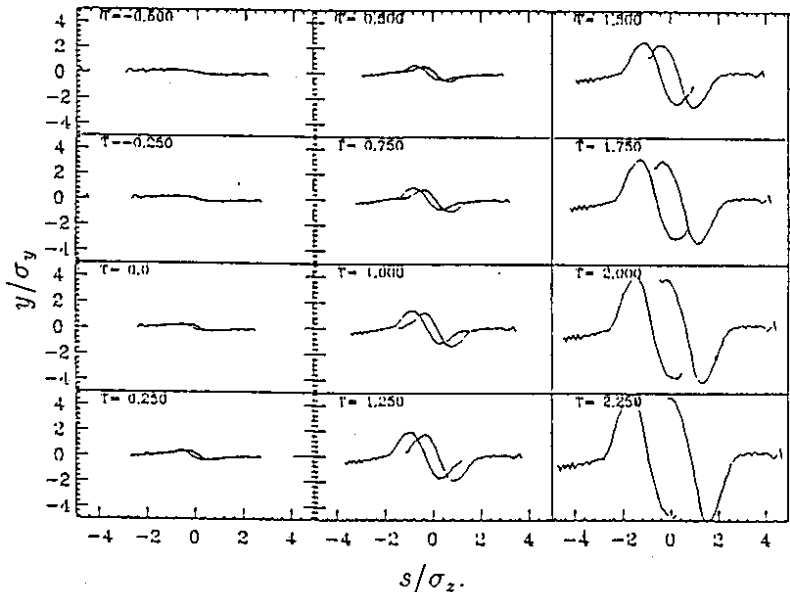
The region of large D and small but non-zero Δ is sensitive to computing errors. We can see in this figure that, when D is large, a tiny offset is enough to degrade the luminosity from the line of vanishing Δ . Therefore, in practice, the enhancement rapidly increases upto ~ 5 with D and then falls off if Δ is sufficiently small but non-zero. This behavior is common to all the simulations so far reported.

Fig.2a and 2b show results for flat beams with $A_y=0.2$ and 1.0 , respectively. We find a similar behavior as that for round beams. The dependence on Δ for large D_y is clearer since we can simulate down to as small a value as $\Delta = 0.1\sigma_y$ because the problem is nearly one-dimensional. A quantitative difference from the round beam case is that we can expect an enhancement at most of factor 2 for flat beams. Therefore, the luminosity enhancement is not a big issue for colliders of the next generation, although some more enhancement might be expected by carefully shaping the longitudinal distribution. The more important is the dependence on the offset Δ , which will be discussed later.

2.4 Kink Instability

The saturation of H_D as a function of D and its subsequent decrease are explained by the effect called kink (or two-stream) instability. Fig.3 shows a typical behavior of the bunches during collision. In each plot corresponding to a different time stage t/σ_z , the vertical center-of-mass coordinate y/σ_y of longitudinal slices is plotted as a function of the longitudinal coordinate s/σ_z . The two beams are initially displaced by $\Delta = 0.2\sigma_y$. ($D_y=20$ is used.) The displacement between the two beams grows in time, causing a loss of luminosity.

Fig.3. Evolution of the kink instability. The beams collide with the initial vertical offset $\Delta_y=0.2\sigma_y$. The time range $0.5 < t < 2.25$ (t in units of σ_z) is shown with the time mesh 0.25. In each plot the vertical center-of-mass y/σ_y is shown as a function of the longitudinal position s/σ_z . Flat beam with $D_y=20$.



This phenomena can be explained by a simple model[7]. Let us model the bunch by a sheet of charge which is uniform in x and z and Gaussian in y . The particle motion for small y can be approximated by

$$\frac{d^2 y_1}{dt^2} = -\omega_0^2 (y_1 - y_2) \quad (\omega_0^2 = \frac{\sqrt{2\pi} D_y}{6 \sigma_z^2}). \quad (2.26)$$

If we transcribe it to the Euler picture $y(s, t)$, we have

$$\left(\frac{\partial}{\partial t} + \frac{\partial}{\partial s}\right)^2 y_1 = -\omega_0^2(y_1 - y_2), \quad \left(\frac{\partial}{\partial t} - \frac{\partial}{\partial s}\right)^2 y_2 = \omega_0^2(y_1 - y_2). \quad (2.27)$$

We easily get a solution in the form

$$y_j = a_j e^{i(k s - \omega t)} \quad (j = 1, 2) \quad (2.28)$$

with

$$\begin{pmatrix} (\omega - k)^2 - \omega_0^2 & \omega_0^2 \\ \omega_0^2 & (\omega + k)^2 - \omega_0^2 \end{pmatrix} \begin{pmatrix} a_1 \\ a_2 \end{pmatrix} = 0, \quad (2.29)$$

which leads to a dispersion relation

$$\omega^2 = k^2 + \omega_0^2 \pm \sqrt{4\omega_0^2 k^2 + \omega_0^4}. \quad (2.30)$$

The solution is unstable if $|k| < \sqrt{2}\omega_0$ and the growth rate is given by

$$|\Im\omega| = [\sqrt{4\omega_0^2 k^2 + \omega_0^4} - (\omega_0^2 + k^2)]^{1/2}. \quad (2.31)$$

The most unstable solution (the largest $\Im\omega$) is

$$k = \pm \frac{\sqrt{3}}{2}\omega_0, \quad \omega = \frac{i}{2}\omega_0$$

$$y_{1(2)} = a_0 \exp\left[\frac{1}{2}\omega_0 t \pm i\left(\frac{\sqrt{3}}{2}\omega_0 s - \frac{\pi}{6}\right)\right] \quad (0 < t < \sqrt{3}\sigma_z). \quad (2.32)$$

The growth factor of the amplitude is $\exp(\sqrt{3}/2\omega_0\sigma_z) = \exp(\sqrt{2\pi}D_y/8)$. This solution can qualitatively explain the phenomena seen in the simulation. For example, eq.(2.32) shows a standing wave behavior w.r.t. s and t , which is clearly seen in Fig.3. Also, the phase difference of 60 degrees between the electron and positron oscillations agrees well with the simulation.

The exponential dependence of the growth factor on the disruption parameter might seem disastrous, but in practice the kink phenomena is actually rather beneficial. For a large enough D_y , even when the initial displacement Δ_y is much larger than σ_y where one expects the luminosity to be exponentially small in the absense of the interaction, the initial stage of the kink instability helps to bring the beam centers closer to give significant luminosity.

If $\sigma_y \ll \Delta_y \ll \sigma_x$, the equation of motion is approximately given by

$$\frac{d^2 y}{dt^2} + \frac{\pi}{6} \frac{\sigma_y D_y}{\sigma_z^2} = 0. \quad (2.33)$$

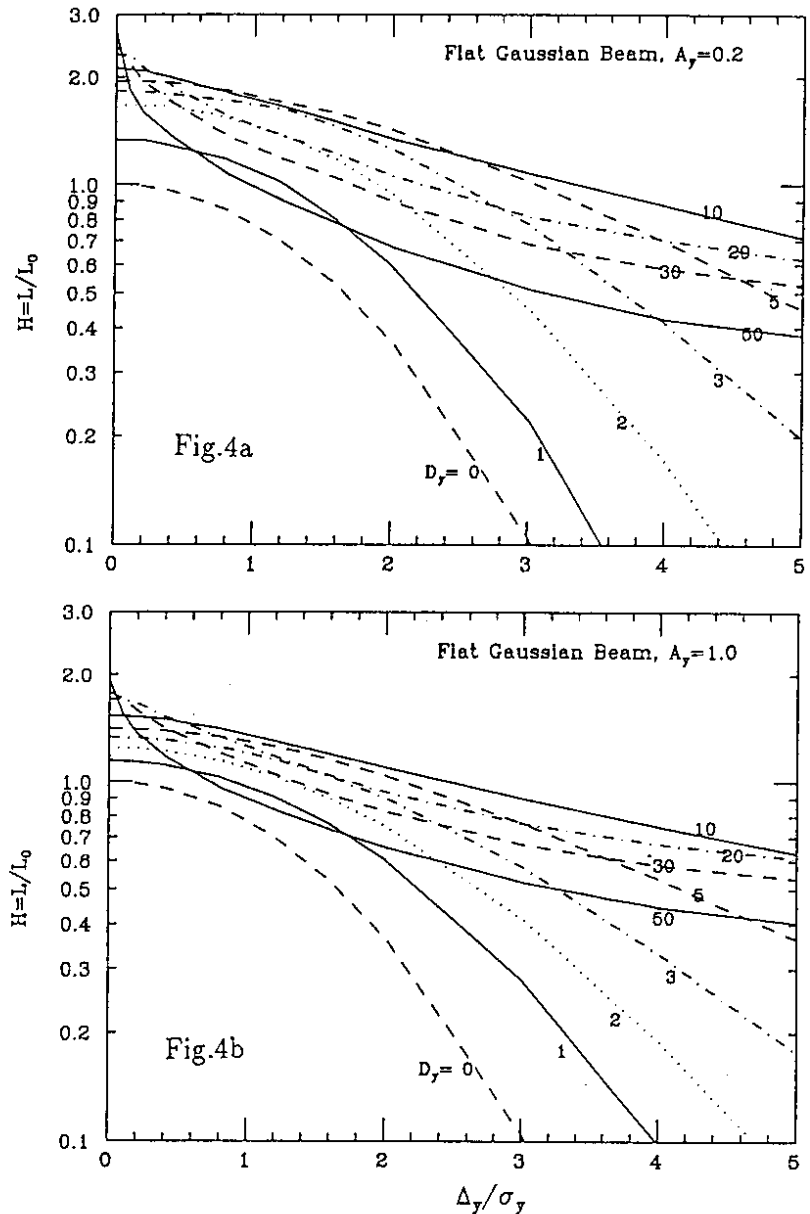
The solution is a parabolic function of t and the two beam centers can overlap in time if

$$\Delta_y \lesssim \frac{\pi}{4} \sigma_y D_y. \quad (2.34)$$

Thus, so long as $\Delta_y/\sigma_y \lesssim D_y$, there is no significant loss of luminosity.

The enhancement factor H_D is plotted in Fig.4 as a function of the initial displacement for various values of D_y . ($A_y=0.2$ and 1.0 in Fig.4a and 4b, respectively.) The curve for $D_y = 0$ shows the analytic formula $\exp(-\Delta_y^2/4\sigma_y^2)$. H_D falls off rapidly when D_y is small. But when D_y is large, H_D sustains within a large range of Δ_y except for a sharp decrease when depart from the situation of perfect alignment. In particular, H_D tends to be most insensitive to the displacement for $5 \lesssim D_y \lesssim 20$ gives. Above this region, the initial drop is too serious.

Fig.4. Enhancement factor H_D vs. initial offset Δ_y for various values of the disruption parameter D_y . Flat Gaussian beam. $A_y=0.2$ in Fig.4a and 1.0 in Fig.4b. An analytic expression is used for the curve $D_y=0$.



2.5 Disruption Angle.

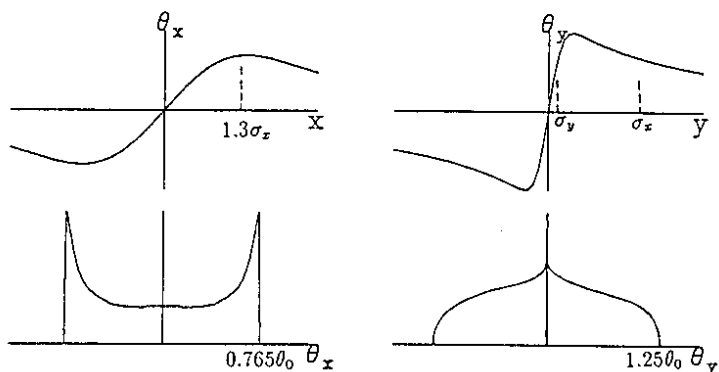
The distribution of the deflection angle is another important issue among the classical effects. It was a major factor in determining the aperture of the final quadrupole magnet in the SLC.

First, let us consider the outgoing angles of the full energy particles. The angle is characterized by the parameter

$$\theta_0 \equiv \frac{2Nr_e}{\gamma(\sigma_x + \sigma_y)} = \frac{D_x\sigma_x}{\sigma_z} = \frac{D_y\sigma_y}{\sigma_z}. \quad (2.35)$$

The horizontal and vertical angles are always comparable but their distributions are very different if the beams are very flat. The outgoing angles as functions of the initial particle position (x_0, y_0) and their distribution is schematically plotted in Fig.5 for flat beams with very small D_y . The horizontal angle θ_x as a function of x_0 has a turning point near $x_0 \sim 1.3\sigma_x$, which gives a cusp in the distribution of θ_x at its maximum $\theta_{x,max} = 0.765\theta_0$. On the other hand the turning point of θ_y is located at large y_0 (infinity if $\sigma_x/\sigma_y \rightarrow \infty$) where the particle density is exponentially small. Therefore, the distribution function of θ_y is small near its maximum $\theta_{y,max} = 1.25\theta_0$. The r.m.s. angles are the same: $\theta_{x,rms} = \theta_{y,rms} = 0.550\theta_0$.

Fig.5. Horizontal and Vertical deflection angles as functions of x and y (top) and their distribution functions (bottom). Flat beams with small disruption parameters.



A simulation result for finite D_y is shown in Fig.6 where $\theta_{y,max}/\theta_0$ (solid curve) and $\theta_{y,rms}/\theta_0$ (dashed curve) are plotted vs. D_y for $A_y=0.2$. The dependence on A_y is weak except for small D_y , where the initial angular spread (truncated at 2.5 sigmas) dominates. The curve for $A_y \rightarrow 0$ can be fitted by

$$\begin{aligned} \theta_{y,rms} &\sim \frac{0.55\theta_0}{[1 + (0.5D_y)^5]^{1/6}} \\ \theta_{y,max} &\sim 2.5\theta_{y,rms}. \end{aligned} \quad (2.36)$$

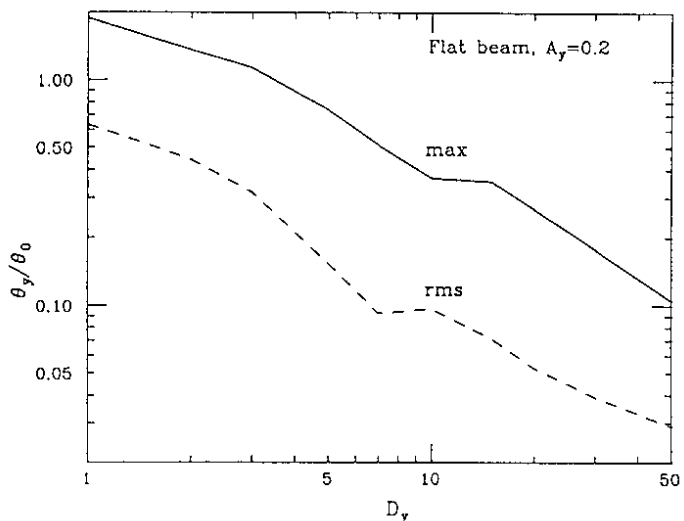


Fig.6. Maximum and r.m.s. disruption angles for a head-on collision of flat beams.

In the next generation colliders we expect the occurrence of particles with energies much lower than the initial beam energy due to processes such as the bremsstrahlung and pair creation. These processes will be discussed in the next section. Here, we discuss the deflection angles of these low energy particles, assuming that they are fewer in number so

that they do not effectively modify the nature of disruption.

Consider a particle with the energy ϵE_0 ($\epsilon \ll 1$). The effective disruption parameter D_x/ϵ and D_y/ϵ can be very large so that the outgoing angle is much larger than that of the full energy particles. The pair creation process always generates oppositely charged particles (e.g., positrons traveling along the same direction as the initial electrons). Their trajectories are very different from those with same sign of charge.

Let us first consider the same charge particles. They are focused by the oncoming beam and oscillate within the beam. The equation of motion is approximately

$$\frac{d^2x}{dt^2} + \frac{D_x}{\epsilon} \frac{x}{\sqrt{3}\sigma_z^2} = 0, \quad (2.37)$$

where, for simplicity, we assume a uniform longitudinal distribution. If the particle is created at the beginning of the collision at $x=x_0$ (we ignore the initial angle), the angle at exit $t=\sqrt{3}\sigma_z$ is

$$\theta_x = -x_0 \sqrt{\frac{D_x}{\sqrt{3}\epsilon\sigma_z}} \frac{1}{\epsilon} \sin \sqrt{\frac{\sqrt{3}D_x}{\epsilon}}. \quad (2.38)$$

Assuming $|x_0| \lesssim \sigma_x$ (the deflection is smaller for $|x_0| \gtrsim \sigma_x$ because of the nonlinearity), we get the maximum horizontal deflection angle

$$\theta_{x,max} \sim \begin{cases} \theta_0/\epsilon & (D_x/\epsilon \lesssim 1/\sqrt{3}) \\ \theta_0/\sqrt{\sqrt{3}\epsilon D_x} & (D_x/\epsilon \gtrsim 1/\sqrt{3}). \end{cases} \quad (2.39)$$

A similar expression holds for the vertical angle but, since D_y is usually larger than 1, we only have the region $D_y/\epsilon \gg 1$:

$$\theta_{y,max} \sim \sqrt{\frac{1}{\sqrt{3}\epsilon D_y}} \theta_0. \quad (2.40)$$

Since $D_y > D_x$, the maximum horizontal angle is larger than the vertical by a factor $\sqrt{D_y/D_x}$ for the same charge particles. The reason is that the vertical oscillation number is larger than the horizontal so that the vertical effect does not accumulate.

Next, consider an oppositely charged particle. In this case the beam-beam force is defocusing and, if D/ϵ is large, the particle can be quickly deflected out of the beam and the effect of the far region $\Phi \sim \log r$ dominates eventually.

Assume a uniform elliptic cylinder distribution. The potential Φ on the line $y=0$ is given by

$$\Phi(x) = \begin{cases} x^2/a_x^2 & (|x| < a_x) \\ \log \frac{|x| + \sqrt{x^2 - a_x^2}}{a_x} + \frac{|x|}{|x| + \sqrt{x^2 - a_x^2}} & (|x| > a_x) \end{cases} \quad (2.41)$$

where $a_x=2\sigma_x$, $a_y=2\sigma_y$ and we assumed $a_x \gg a_y$. The equation of motion can be integrated once and gives

$$\frac{1}{2} \dot{x}^2 = \frac{D_x \sigma_x^2}{\sqrt{3}\epsilon \sigma_z^2} [\Phi(x) - \Phi(x_0)] \quad (0 < t < \sqrt{3}\sigma_z) \quad (2.42)$$

By approximately solving this equation, we find the maximum deflection angle to be

$$\theta_{x,max} \sim \begin{cases} \theta_0/\epsilon & (D_x/\epsilon \lesssim 1) \\ \left[\log(4\sqrt{3}D_x/\epsilon)/(\sqrt{3}\epsilon D_x) \right]^{1/2} \theta_0 & (D_x/\epsilon \gtrsim 1). \end{cases} \quad (2.43)$$

The potential Φ on the line $x = 0$ is given by

$$\Phi(y) = \begin{cases} y^2/a_x a_y & (|y| < a_y) \\ \log \frac{|y| + \sqrt{y^2 + a_x^2}}{a_x} + \frac{|y|}{|y| + \sqrt{y^2 + a_x^2}} & (|y| > a_y) \end{cases} \quad (2.44)$$

If $D_y/\epsilon \gtrsim 1$, the contribution of the region $|y| < a_y$ is negligible, and we get the same approximate expression for θ_y as for θ_x regardless of D_x/ϵ . Thus, so long as $D_y/\epsilon \gg 1$, three angles $\theta_{x,same}$, $\theta_{x,opp}$ and $\theta_{y,opp}$ are comparable apart from the logarithmic factor $\log(D_x/\epsilon)$ and $\theta_{y,same}$ are much smaller than these.

2.6 Center-of-Mass Deflection

If the bunches are displaced transversely before collision, the center-of-mass of the bunches is deflected by the beam-beam force. The relation between the initial displacement $\Delta_{x,y}$ and the center-of-mass deflection angle $\Theta_{x,y}$ is useful for monitoring the beam position. For small displacement and small disruption, $\Theta_{x(y)}$ is given by $\frac{1}{2} \theta_0 \Delta_{x(y)}/\sigma_{x(y)}$. The relation between Δ and Θ is plotted schematically in Fig.7 for very flat beams. Θ_x has a maximum near $\sim \sigma_x$ whereas Θ_y is almost flat in a wide range $\sigma_y < \Delta_y < \sigma_x$. In general, we define the form factor F for the vertical deflection by

$$\Theta_y = \frac{1}{2} \theta_0 F(\Delta_y/\sigma_y). \quad (2.45)$$

For small D_y , F is given by

$$\begin{aligned} F(\delta) &= \frac{1}{\sqrt{\pi}} \int_0^\delta d\tau \int_{-\infty}^\infty d\xi \frac{1}{\sqrt{1 + A_y^2 \xi^2}} e^{-\xi^2 - \tau^2/4/(1 + A_y^2 \xi^2)} \\ &= \int_0^\delta d\tau e^{-\tau^2/4} \quad (A_y = 0) \\ &= \delta/(1 + A_y^2/4) \quad (\delta \rightarrow 0, A_y \rightarrow 0), \quad = \sqrt{\pi} \quad (\delta \rightarrow \infty). \end{aligned} \quad (2.46)$$

The dependence on A_y is small as long as $A_y \lesssim 1$.

The form factor F for finite D_y obtained by simulations is plotted in Fig.8. When D_y is small, Θ_y saturates at a few σ_y . If, therefore, Δ_y is large, the deflection does not have information about Δ_y and cannot be used as a sensitive position monitor. However, when D_y is large, say 10, the deflection measurement can be useful even for $\Delta_y \gtrsim 5\sigma_y$.

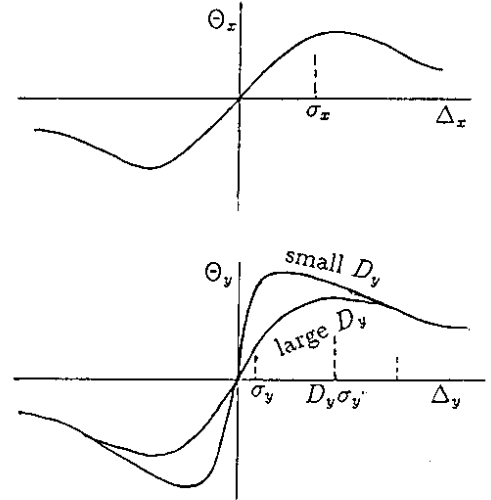
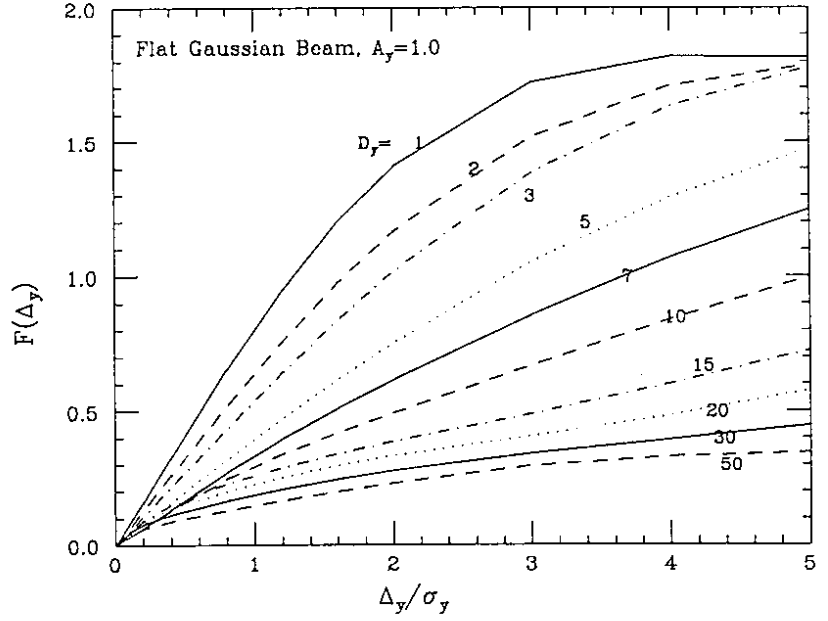


Fig.7. Center-of-mass deflection as a function of the displacement.

Fig.8. The form factor F of the center-of-mass deflection angle as a function of the initial offset Δ_y and the disruption parameter D_y . Flat beam with $A_y=1.0$.



Multibunch crossing instability

When a beam pulse consists of several bunches, there can be undesired close encounters of bunches before and after the central collision point. Let us consider this peripheral interaction in the case of flat beams with a horizontal crossing angle. (The multi-bunch head-on scheme seems to be unpractical.)

The second electron bunch before collision is attracted by the first positron bunch at a distance after the first collision. As a result the former arrives at the collision point with a horizontal displacement. This effect gives the same horizontal displacement for the second positron bunch. Thus the second collision will take place at a collision point which is slightly shifted horizontally but with no relative offset.

However, this is not true if there is a vertical displacement due to errors somewhere upstream[8]. If the vertical shift of the first electron bunch is positive, for example, it will kick the first positron upwards at the central collision point and itself is kicked downwards. Consequently, this electron bunch will, at peripheral encounters, kick downwards all the following positron bunches, which, in turn, will arrive at the collision point with negative displacements. Thus, all the effects add up with opposite signatures between electrons and positrons to cause an instability. This phenomena is physically the same mechanism as the kink instability discussed before, albeit that it is manifested in a discrete form.

Let us denote the vertical offset of the k -th e^\pm bunch in units of σ_y by Δ_k^\pm . Then, the l -th e^\mp bunch is kicked by the l -th e^\pm bunch at the collision point by an angle $y_l' = \frac{1}{2} \theta_0 F(\Delta_l^\pm - \Delta_l^\mp)$. When this bunch encounter the k -th ($k > l$) e^\pm bunch, the latter is kicked vertically by an angle $2Nr_c/\gamma \times y_l' L_{k,l}/(L_{k,l}\phi_c)^2$. Here, $L_{k,l}$ is the distance between the central collision point and the encounter point of the k -th and l -th bunches and ϕ_c is the crossing angle. Therefore, $L_{k,l}\phi_c$ is the distance of encounter. (We assume $L_{k,l}\phi_c \gg \sigma_x$.) After this encounter, the k -th e^\pm bunch travels a distance $L_{k,l}$ till the collision. Therefore, the vertical shift of the k -th bunch due to this encounter is given

by $Nr_e\theta_0/(\gamma\phi_c^2)F(\Delta_l^\pm - \Delta_l^\mp)$, which is independent of $L_{k,l}$. Thus, denoting the relative displacement by $\Delta_k \equiv \Delta_k^+ - \Delta_k^-$, we obtain

$$\Delta_k = C \sum_{l=1}^{k-1} F(\Delta_l) + \Delta_{k,0}, \quad C = D_x D_y \left[\frac{\sigma_x/\sigma_z}{\phi_c} \right]^2 = \frac{D_x D_y}{c_\phi^2} \quad (2.47)$$

where $\Delta_{k,0}$ is the displacement due to errors upstream.

If $\Delta_{k,0}=\Delta_0$ for all the bunches and if D_y and Δ are small so that $F(\Delta) \sim \Delta$, we get

$$\Delta_k = (1 + C)^{k-1} \Delta_0. \quad (2.48)$$

Therefore, this effect is serious if $C(m_b - 1) \gtrsim 1$ where m_b is the number of bunches which encounter. However, this criterion is too pessimistic because, as we can see in Fig.8, $F(\Delta)$ is considerably smaller than Δ if D_y is large.

By converting eq.(2.47) into a differential equation w.r.t. k , we can approximately solve the equation. Then the criterion of tolerable instability becomes

$$C(m_b - 1) \lesssim \int_{\Delta_0}^{\Delta_{fin}} \frac{d\Delta}{F(\Delta)} \quad (2.49)$$

where Δ_{fin} is the maximum tolerable displacement of the last bunch. Because $F(\Delta)$ is not linear in Δ , the criterion depends both on Δ_0 and Δ_{fin} . The function on the r.h.s. is plotted in Fig.9 as a function of D_y for $A_y=1.0$. Two curves correspond to $(\Delta_0, \Delta_{fin}) = (0.2, 0.4)$ (dashed line) and $(0.5, 1.0)$ (solid line), respectively.

The latter range of Δ seems to be more practical. Thus, the criterion that the blow-up factor is to be less than two is given by

$$C(m_b - 1) \lesssim \sqrt{\frac{1}{2} + \frac{D_y}{3}} \quad (2.50)$$

which is shown by the dotted line in Fig.9.

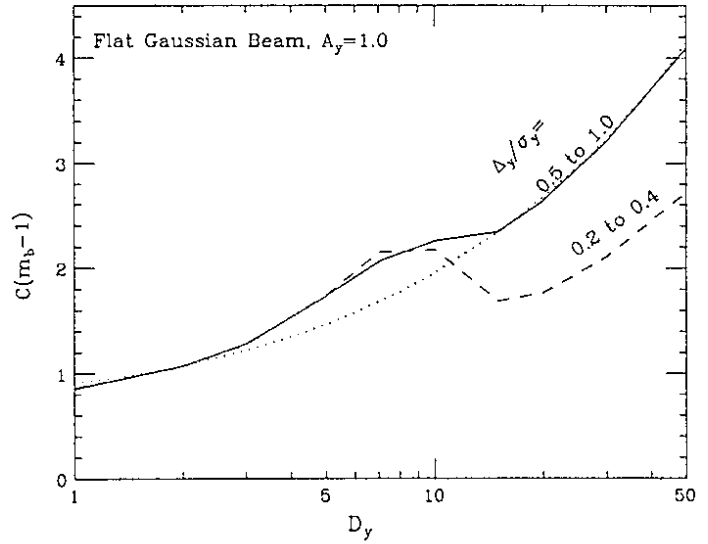


Fig.9. Criterion for the multibunch crossing instability.

3 Quantum Beamstrahlung

The magnetic field in the bunch during collision is typically of the order of kilo-Teslas in the linear colliders of the next generation. Therefore, even though the longitudinal length of the field is small $\sim \sigma_z \sim 10^{-4}\text{m}$, the synchrotron radiation, called beamstrahlung in this case, plays an important role. As we shall see later, the so-called radiation coherence length $l_R \approx \rho/\gamma$, ρ being the orbit radius of curvature, is typically $\sim 10^{-6}\text{m}$, which is considerably smaller than the bunch length. (When the disruption parameter is large, the field seen by a particle changes within a longitudinal distance $\sim \sigma_z/\sqrt{D}$. But l_R is usually still smaller than this length though a bit marginally.) Therefore, we can invoke the formula of the synchrotron radiation in a constant field.

The radiation is characterized by the critical energy ω_c . Let us introduce the dimensionless, Lorentz invariant parameter Υ , defined by

$$\Upsilon \equiv \frac{2\hbar\omega_c}{3E} = \frac{\lambda_e\gamma^2}{\rho} = \gamma\frac{B}{B_c} = \frac{e}{m^3}\sqrt{|(F_{\mu\nu}p^\nu)^2|} \quad (3.51)$$

where E is the electron energy before radiation, λ_e the Compton wave length, $F_{\mu\nu}$ the energy-momentum tensor of the field, p^ν the 4-momentum of the electron, B the magnetic field (actually, $|\mathbf{E}| + |\mathbf{B}|$) and B_c the critical magnetic field defined as $B_c = m^2/e \approx 4.4$ GTeslas. (The parameter $\xi \equiv \omega_c/E = 3\Upsilon/2$ is also often adopted instead of Υ .)

This parameter Υ is not a constant during the collision. In the case of Gaussian beams, the maximum and average of its value can be estimated by

$$\Upsilon_{max} \approx \frac{2Nr_e^2\gamma}{\alpha\sigma_z(\sigma_x + \sigma_y)}, \quad \Upsilon_{avr} \approx \frac{5}{12}\Upsilon_{max} \quad (3.52)$$

where α is the fine structure constant. The SLC design parameters give $\Upsilon_{avr} \sim 0.004$. In the linear colliders of the next generation we will have $\Upsilon_{avr} \sim 0.1$ to 1.0 , i.e., the typical photon energy is comparable to the initial electron energy. Therefore, we need to take into account the recoil of the electron. We cannot use the standard radiation formula used in storage ring theories, and the quantum electrodynamic (QED) formulation is necessary.

3.1 Sokolov-Ternov Formula

The radiation formula for arbitrary Υ was first derived by Sokolov and Ternov[9]. They used the exact solution of the Dirac equation in a uniform magnetic field and computed the transition rate. Baier and Katkov[10] rederived the same formula by a method which is very powerful for general semi-classical problems such as the radiation in varying fields. Here, we shall follow the latter.

The matrix element for one photon emission with momentum \mathbf{k} and energy $\omega = |\mathbf{k}|$ is written in the form

$$\left\langle f \left| \frac{e}{\sqrt{2\omega}} \int dt e^{i\omega t} M(t) \right| i \right\rangle, \quad M(t) = u_s^\dagger \boldsymbol{\alpha} \cdot \boldsymbol{\varepsilon} e^{-i\mathbf{k}\cdot\mathbf{x}(t)} u_s$$

where $s(s')$ is the initial (final) electron spin state, $\boldsymbol{\varepsilon}$ the photon polarization vector, $\boldsymbol{\alpha}$ the Dirac matrix, and $\mathbf{x}(t)$ the Heisenberg position operator. The probability of the photon

emission is given by

$$dw_\gamma = \frac{e^2}{4\pi} \frac{d\mathbf{k}}{(2\pi)^2 \omega} \left\langle i \left| \int dt_1 dt_2 e^{i\omega(t_1-t_2)} M^\dagger(t_2) M(t_1) \right| i \right\rangle. \quad (3.53)$$

Baier and Katkov reduced this expression into the following form assuming that the electron's dynamical variables commute (treat the electron orbit classically) but retaining the commutator between electron and photon variables (take into account the recoil):

$$dw_\gamma = \frac{e^2}{4\pi} \frac{d\mathbf{k}}{(2\pi)^2 \omega} \int dt_1 dt_2 \exp i\left[\omega(t_1 - t_2) - \frac{E}{E - \omega} \mathbf{k} \cdot (\mathbf{x}(t_1) - \mathbf{x}(t_2))\right] R^*(t_2) R(t_1) \quad (3.54)$$

where

$$R(t) = \varphi_f^* \left[\frac{1}{2} \boldsymbol{\varepsilon} \cdot \mathbf{p} \left(\frac{1}{E_{\mathbf{p}} + m} + \frac{1}{E_{\mathbf{p}'} + m} \right) + \frac{1}{2} \left(\frac{\boldsymbol{\varepsilon} \times \mathbf{p}}{E_{\mathbf{p}} + m} - \frac{\boldsymbol{\varepsilon} \times \mathbf{p}'}{E_{\mathbf{p}'} + m} \right) \right] \varphi_i.$$

Here, φ 's are the 2-component spinors and $\mathbf{p} = E\mathbf{v}(t)$, $\mathbf{p}' = \mathbf{p} - \mathbf{k}$, $E_{\mathbf{p}} = \sqrt{m^2 + \mathbf{p}^2}$, $E_{\mathbf{p}'} = \sqrt{m^2 + \mathbf{p}'^2}$. In these expressions all the variables are already c-numbers. Thus, $\mathbf{x}(t)$ is the classical electron trajectory and $\mathbf{v}(t) = d\mathbf{x}/dt$. Summing over the final spins and photon polarizations and averaging over the initial spins, one can replace R^*R with

$$\left(1 + \frac{\omega}{E'} + \frac{1}{2} \frac{\omega^2}{E'^2} \right) [\mathbf{v}(t_1) \cdot \mathbf{v}(t_2) - 1] + \frac{1}{2\gamma^2} \frac{\omega^2}{E'^2}, \quad E' = E - \omega.$$

Let us define $t_{1(2)} = t \mp \tau/2$. When the field variation length ($\sim \min(\sigma_z, \sigma_z/\sqrt{D})$) is small compared with l_R , we can expand the integrand in terms of τ . To get the constant field formula, the following terms are enough.

$$\mathbf{v}(t_1) \cdot \mathbf{v}(t_2) - 1 = -\frac{1}{\gamma^2} - \frac{1}{2} |\dot{\mathbf{v}}(t)|^2 \tau^2, \quad \mathbf{x}(t_2) - \mathbf{x}(t_1) = \mathbf{v}(t)\tau + \frac{1}{24} \ddot{\mathbf{v}}(t)\tau^3.$$

By integrating eq.(3.54) over the photon angle $\mathbf{k}/|\mathbf{k}|$ we get

$$\frac{dW_\gamma}{d\omega} = \frac{ie^2}{8\pi^2} \frac{E'}{E} \int_{-\infty}^{\infty} \frac{d\tau}{\tau - i0} \left[\frac{1 + \frac{\omega}{E'}}{\gamma^2} + \left(1 + \frac{\omega}{E'} + \frac{1}{2} \frac{\omega^2}{E'^2} \right) \frac{\tau^2}{2\rho^2} \right] \exp \left[-i \frac{\omega}{E' \Upsilon} \frac{\gamma \tau}{2\rho} \left[1 + \frac{1}{3} \left(\frac{\gamma \tau}{2\rho} \right)^2 \right] \right] \quad (3.55)$$

where $1/\rho = |\dot{\mathbf{v}}(t)|$ and $W_\gamma = dw_\gamma/dt$.

The range of τ which gives a significant contribution to the integral is called radiation coherence length l_R . Note that, in the integration like $\int dx \exp[-ic(x + x^3/3)]$, the significant contribution comes from the region $|x| \lesssim c^{-1/3}$ when $c \ll 1$ (x^3 term) and from $|x| \lesssim c^{-1/2}$ when $c \gg 1$ (saddle point of the phase). Therefore, the radiation coherence length is

$$l_R \approx \frac{\rho}{\gamma} \left[\frac{\omega}{E - \omega \Upsilon} \frac{1}{\Upsilon} \right]^{-1/3}, \quad \left(\frac{\omega}{E - \omega \Upsilon} \frac{1}{\Upsilon} \ll 1 \right); \quad \approx \frac{\rho}{\gamma} \left[\frac{\omega}{E - \omega \Upsilon} \frac{1}{\Upsilon} \right]^{-1/2}, \quad \left(\frac{\omega}{E - \omega \Upsilon} \frac{1}{\Upsilon} \gg 1 \right). \quad (3.56)$$

In the case $\Upsilon \ll 1$, as in storage rings, for most photons $\omega/\Upsilon E$ is $O(1)$ which gives $l_R \approx \rho/\gamma$. (This is not true for photons with energies much lower than the critical energy.)

For such radiation we need to use $l_R \approx (\rho/\gamma)(\omega_c/\omega)^{1/3}$. When Υ is large, the coherence length is $l_R \approx (\rho/\gamma)\Upsilon^{1/3}$ because $\omega/(E - \omega)$ is $O(1)$. For the next generation linear colliders, in which Υ is $O(1)$, we can ignore the factor $\Upsilon^{1/3}$.

Now, by using the formulas

$$\int_{-\infty}^{\infty} \frac{1}{x - i0} e^{-ic(x+x^3/3)} dx = \frac{2i}{\sqrt{3}} \int_{2c/3}^{\infty} K_{1/3}(x) dx$$

$$\int_{-\infty}^{\infty} x \sin c(x + \frac{x^3}{3}) dx = \frac{1}{\sqrt{3}} K_{2/3}(\frac{2c}{3})$$

where K_ν is the modified Bessel function, we obtain the Sokolov-Ternov spectrum formula

$$\frac{dW_\gamma}{d\omega} = \frac{\alpha}{\sqrt{3}\pi\gamma^2} F_{BS} \quad (3.57)$$

with

$$F_{BS} = - \int_{\xi}^{\infty} K_{1/3}(\xi') d\xi' + \left(\frac{E - \omega}{E} + \frac{E}{E - \omega} \right) K_{2/3}(\xi) \quad (3.58)$$

$$= \int_{\xi}^{\infty} K_{5/3}(\xi') d\xi' + \frac{y^2}{1 - y} K_{2/3}(\xi), \quad (3.59)$$

where

$$\xi = \frac{2\omega}{3\Upsilon(E - \omega)} = \frac{\omega}{\omega_c} \frac{1}{1 - \omega/E} = \frac{2}{3\Upsilon} \frac{y}{1 - y}, \quad (y = \frac{\omega}{E}). \quad (3.60)$$

In the classical limit $\Upsilon \rightarrow 0$ the second term in eq.(3.59) can be ignored and we come to the classical spectrum formula.

The Sokolov-Ternov power spectrum is schematically shown in Fig.10. The low energy behavior $P(\omega) \propto \omega^{1/3}$ is the same as the classical formula. The high energy part extends to infinite (unphysical) energy as $\exp(-\omega/\omega_c)$ in the classical formula but it is truncated at $\omega = E$ in the Sokolov-Ternov formula. The high energy tail is expressed as $e^{-\xi}$. In the log-log plot, the spectrum approaches nearly a triangular form in the limit $\Upsilon \rightarrow \infty$.

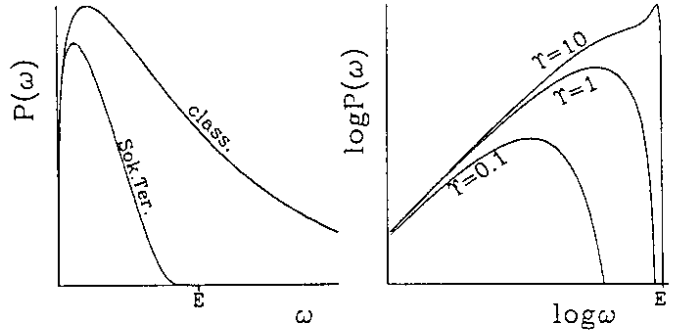


Fig.10. Sokolov-Ternov Spectrum Function

3.2 Number of Photons and Average Energy Loss

By integrating eq.(3.58) over the photon energy, we obtain the expected number of photons per unit time:

$$\frac{dN_\gamma}{dt} = \int_0^E \frac{dW_\gamma}{d\omega} d\omega = \frac{5}{2\sqrt{3}} \frac{\alpha\Upsilon}{\lambda_e\gamma} \cdot U_0(\Upsilon) \quad (3.61)$$

with

$$U_0(\Upsilon) = \left\{ \begin{array}{l} 1 \quad (\Upsilon \rightarrow 0) \\ \frac{28\sqrt{3}}{45}\Gamma(2/3)(3\Upsilon)^{-1/3} = 1.012\Upsilon^{-1/3} \quad (\Upsilon \rightarrow \infty) \end{array} \right\} \approx \frac{1}{(1 + \Upsilon^{2/3})^{1/2}}. \quad (3.62)$$

The average energy loss per unit time is

$$\left\langle -\frac{1}{E} \frac{dE}{dt} \right\rangle = \int_0^\infty \frac{\omega}{E} \frac{dW_\gamma}{d\omega} d\omega = \frac{2}{3} \frac{\alpha \Upsilon^2}{\lambda_e \gamma} \cdot U_1(\Upsilon) \quad (3.63)$$

with

$$U_1(\Upsilon) = \left\{ \begin{array}{l} 1 \quad (\Upsilon \rightarrow 0) \\ \frac{16}{9}\Gamma(2/3)(3\Upsilon)^{-4/3} = 0.556\Upsilon^{-4/3} \quad (\Upsilon \rightarrow \infty) \end{array} \right\} \approx \frac{1}{[1 + (1.5\Upsilon)^{2/3}]^2}. \quad (3.64)$$

The functions U_0 and U_1 are plotted in Fig.11.

The average photon energy is

$$\begin{aligned} \frac{\langle \omega \rangle}{E} &= \frac{4\sqrt{3}}{15} \Upsilon \frac{U_1(\Upsilon)}{U_0(\Upsilon)} \quad (3.65) \\ &= \begin{cases} 0.462\Upsilon & (\Upsilon \rightarrow 0) \\ \frac{16}{63} = 0.254 & (\Upsilon \rightarrow \infty) \end{cases} \end{aligned}$$

Note that the average photon energy is finite (about one quarter of the initial energy) in the limit $\Upsilon \rightarrow \infty$.

In the case of a collision of Gaussian bunches, the average number of emitted photons per electron n_γ and the relative energy loss δ_E can be given approximately by

$$n_\gamma \approx 1.06\alpha r_e N \frac{2}{\sigma_x + \sigma_y} U_0(\Upsilon_{avr}) \approx 2.54 \left[\frac{\alpha \sigma_z \Upsilon_{avr}}{\lambda_e \gamma} \right] U_0(\Upsilon_{avr}) \quad (3.66)$$

$$\delta_E = \left\langle -\frac{\Delta E}{E} \right\rangle \approx 0.216 \frac{r_e^3 N^2 \gamma}{\sigma_z} \left(\frac{2}{\sigma_x + \sigma_y} \right)^2 U_1(\Upsilon_{avr}) \approx 1.24 \left[\frac{\alpha \sigma_z \Upsilon_{avr}}{\lambda_e \gamma} \right] \Upsilon_{avr} U_1(\Upsilon_{avr}) \quad (3.67)$$

The beamstrahlung causes a spread in the center-of-mass energy of e^+ and e^- . This effect is characterized by the parameter δ_E . Although it is smaller than 0.1% in the SLC, it is a severe limiting factor for the performance of colliders in the future. As seen in Fig.11, $\Upsilon U_1(\Upsilon)$ is almost constant (0.1 to 0.2) in the wide range $0.2 < \Upsilon < 200$. Therefore, in order to keep δ_E below 10 to 20%, most designs choose $\alpha \sigma_z \Upsilon / \lambda_e \gamma$ around unity. Since U_0 is not far from unity unless Υ is very large, n_γ is also of order unity. It should be noted that the ratio of l_R to σ_z is approximately equal to α/n_γ , which means l_R/σ_z is about 10^{-2} if $n_\gamma \sim 1$.

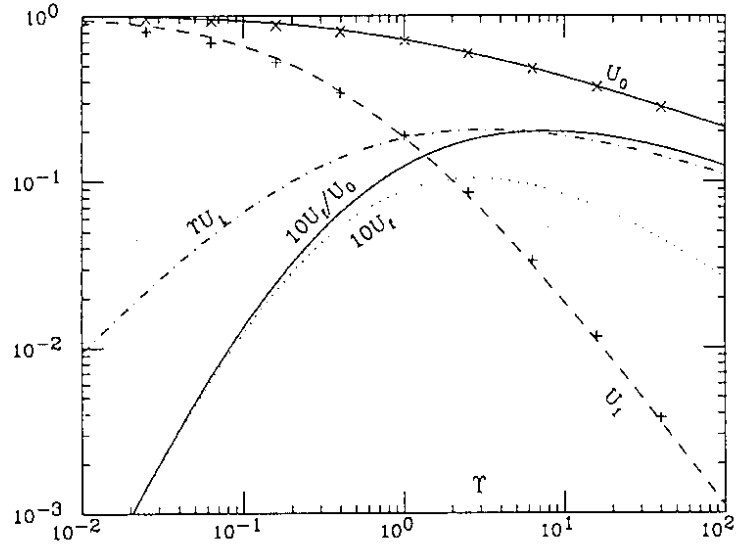


Fig.11. Functions U_0 , U_1 and U_f . The crosses are the approximate formulas in (3.62) and (3.64).

3.3 Energy Spectrum of Electrons

The beamstrahlung alters the energy spectrum of electrons. The final spectrum is complicated in general because of the possibility of emitting more than one photon. If $n_\gamma \ll 1$, however, we may ignore the multi-photon emission. The final electron spectrum is then given approximately by

$$\psi_{fin}(x) = e^{-n_\gamma} \delta(x-1) + (1 - e^{-n_\gamma}) f(1-x) \quad (3.68)$$

where δ is the Dirac delta function (the energy spread before collision is negligible) and $f(y)$ is the Sokolov-Ternov spectrum function normalized as $\int f(y) dy = 1$. Υ in $f(y)$ may be replaced by the average value. A more detailed calculation is given in [11]. But eq.(3.68) is sufficient as a coarse approximation to be used in background estimations, if $n_\gamma \lesssim 1$.

For the average spectrum we may replace n_γ with $n_\gamma \tau$ ($0 < \tau < 1$) and average over τ :

$$\psi_{avr}(x) \sim \int_0^1 \psi_{fin}(x, n_\gamma \tau) d\tau = \frac{1 - e^{-n_\gamma}}{n_\gamma} \delta(x-1) + \left(1 - \frac{1 - e^{-n_\gamma}}{n_\gamma}\right) f(1-x). \quad (3.69)$$

Simulation results show that the 2-dim differential luminosity spectrum $dL/dx_1 dx_2 = L \times \psi_2(x_1, x_2)$ factorizes quite well as $\psi_{avr}(x_1) \psi_{avr}(x_2)$. Therefore, the center-of-mass spectrum is approximately given by

$$\psi_s(s) \sim \int dx_1 dx_2 \delta(s/4E_0^2 - x_1 x_2) \psi_{avr}(x_1) \psi_{avr}(x_2). \quad (3.70)$$

Actually, 2-dim spectrum is dominated by the two edges $x_1 = 1$ and $x_2 = 1$, i.e., the case where one of the colliding particles is at full energy. Therefore, the events with low s ($\ll 4E_0^2$) go mostly forward along with one of the two beams.

3.4 How to Reduce Beamstrahlung

Since the energy loss due to the beamstrahlung is a big limitation for high energy linear colliders, several methods of reducing it have been investigated.

Short Bunches

As we can see in eq.(3.67), we can reduce δ_E by using a longer bunch in the classical regime $\Upsilon \ll 1$. This is limited, however, by other constraints in colliders such as the control of the energy spread in the linac. In the extreme quantum regime $\Upsilon \gg 1$, δ_E is proportional to $\sigma_z^{-1/3}$ owing to the Υ -dependence of U_1 . This does not help unless Υ is extremely large. The Υ -dependence of δ_E is like $\Upsilon U_1(\Upsilon)$ which is plotted in Fig.11. It is almost flat in the region $0.2 \sim \Upsilon \sim 100$ which is the region for linear colliders of next and, probably, next to next generation.

Another possibility is that, when we go to very short bunch lengths comparable to l_R , the radiation might be suppressed. The radiation by very short bunches has been discussed by many authors [12]. It is concluded, however, that the correction to the constant field formula is small for Gaussian bunches.

Flat Beams

If we go to very flat beams $R = \sigma_x/\sigma_y \rightarrow$ large with fixed area $\sigma_x\sigma_y$, we can reduce $\delta_E \propto R/(1+R)^2$ without sacrificing the luminosity. This is the most practical cure for the next generation colliders. Recent designs mostly adopt flat beams with $R \sim 10$ for CLIC, $R \sim 100$ for NLC and JLC, or even 3000 for VLEPP. It has been demonstrated that flat beams have many other advantages[13], but the price to pay is that the vertical tolerances in the damping ring, the linac and the final focus system become tighter.

Charge Compensation

If each beam is a charge-neutral mixture of electrons and positrons, then the beamstrahlung can in principle be completely suppressed. Apart from the technical difficulties of mixing beams, it was shown[15,16] that the system of the four beams is unstable when the mixing is not perfect. Fig.12a shows the luminosity enhancement factor H_D as a function of the residual charge $\Delta Q/Q$. When $n_y (= \sqrt{D_y}/2\pi)$ exceeds ~ 1 , imperfection of 0.1% is enough to degrade the luminosity. Fig.12b shows $H_D(n_y)$ for two values of the center-of-mass shift Δ_y/σ_y between e^+ and e^- in the same beam. Even a small shift of 1% has a serious effect. Thus, the charge compensation scheme is very hard to realize.

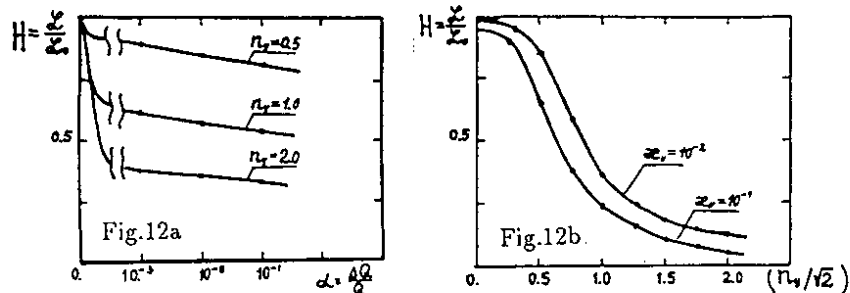


Fig.12. Luminosity enhancement factor in charge compensation scheme. The effect of inaccurate charge compensation (Fig.12a) and that of the shift of one of the beams (Fig.12b). Taken from [15].

Plasma Return Current

During the collision the charges of e^+ and e^- cancel each other but the currents add. If there is a plasma at the collision point, this current may be neutralized by the plasma return current[14]. However, there is a problem of hadronic backgrounds due to the collision with ions.

γ - γ Colliders

If everything fails, we can give up e^+e^- colliders. There is a promising proposal of converting an electron collider into a γ - γ collider. Irradiating an intense laser beam on electrons just before the collision point, we can convert the electrons into photons by the Compton back-scattering. High energy, highly focused photon beams can be produced this way. There is, however, a different constraint on the γ - γ colliders, associated with the "coherent pair creation" (to be discussed in the next section)[17]. The present status of study is summarized in[18].

3.5 Spin-Flip Radiation

It is relatively easier to have longitudinally polarized electrons in linear colliders than in storage rings. It is also possible to have polarized positrons by using polarized photons generated in helical wigglers[19]. There is no major difficulty in preserving the polarization from the source to the collision point. Here, we mention possible depolarizations due to

the beam-beam interaction.

In storage rings electron/positron beams tend to polarize (transversely) due to the spin-flip radiation. The ratio of the spin-flip radiation to the total radiation is very small: $\sim \Upsilon^2 \sim 10^{-11}$ in storage rings. This ratio is much larger in the beam-beam interaction in linear colliders. It is given by

$$\frac{dN_{\gamma,flip}}{dt} = \frac{dN_{\gamma}}{dt} U_{f0}(\Upsilon) \quad (3.71)$$

where the function $U_{f0} = U_f/U_0$ is plotted in Fig.11. The depolarization is given by $\Delta P = 2n_{\gamma}U_{f0}$. As seen in Fig.11, U_{f0} is almost constant in the region $1 \lesssim \Upsilon \lesssim 100$ and does not exceed 0.02. Therefore, if $n_{\gamma} \sim 1$ the depolarization is less than a few percent.

There is another mechanism of depolarization, i.e., due to the classical precession in the magnetic field. The depolarization by this effect was estimated[20] to be $\sim 0.006(n_{\gamma}/U_0)^2$, which is also less than a few percent if $n_{\gamma} \lesssim 3$.

3.6 Bremsstrahlung

The beamstrahlung is produced by the interaction between e^{\pm} and the collective beam-beam field. There are of course photons emitted by the collisions of individual particles, namely the bremsstrahlung $e^+e^- \rightarrow e^+e^-\gamma$. The total crosssection is

$$\sigma_{brems} \approx \frac{1}{2} \frac{16}{3} \alpha r_e^2 [\log 4\gamma^2]^2 \times \left\{ \frac{\log \sigma_y/\lambda_e}{\log 4\gamma^2} \right\} \sim 10^{-24} \text{cm}^2 \quad (3.72)$$

where the factor in the curly brackets is the correction due to the finite beam size[21](see Sec.4.2.4 for more details). We count the photons parallel to one of the incident beams only, which gives the factor 1/2. With the typical luminosity per collision 10^{30}cm^{-2} , we have $\sim 10^6$ photons per collision, which is much smaller than the beamstrahlung.

The energy spectrum is

$$\frac{d\sigma_{brems}}{dy} = \frac{1}{2} \frac{16}{3} \frac{\alpha r_e^2}{y} \left[(1 - y + \frac{3}{4}y^2) \left(\log \frac{\sqrt{2}\sigma_y}{\lambda_e} - \frac{1 + \gamma_E}{2} \right) - \frac{3}{4} \left(\frac{13}{9} - \frac{13}{9}y + y^2 \right) \right] \quad (3.73)$$

where $y = \omega/E$ and $\gamma_E=0.577$ is the Euler's constant. This can exceed the beamstrahlung only at the high energy end $y \sim 1$. The number of low energy final electrons with the energy below xE ($x \ll 1$) is $\sim 10^4 x$ per collision if the luminosity per collision is 10^{30}cm^{-2} .

4 Electron-Positron Pair Creation

In general, low energy electrons and positrons comoving with the e^+e^- beams during collision is a source of deleterious backgrounds. Being lower in energy, these particles can either be deflected more severely by the beam-beam field, or even carry an inherently large angle and transverse momentum, such that they escape from exiting through the exhaust port and pollute the detector. One such source of low energy particles comes directly from the result of beamstrahlung or bremsstrahlung, as described in the last section. A more severe source, however, comes from the second order quantum electrodynamic (QED) process of e^+e^- pair creation during the collision. In this case, there is always one particle in the pair that carries the same sign of charge as the oncoming beam, and will be severely deflected unbound. At lower energies, the pairs are made essentially by the *incoherent* process, where the pair is created by the interaction of particles on the individual particles in the oncoming beam, e.g., the interaction of beamstrahlung photons on the oncoming electrons. This problem was first identified by Zolotarev *et al.*[22].

At energies where the beamstrahlung parameter Υ lies approximately in the range $0.5 \lesssim \Upsilon \lesssim 100$, pair creation from the beamstrahlung photons is dominated by the *coherent* process, first noted by Chen[23]. In this case the photon turns into an e^+e^- pair by interacting with the collective field of the oncoming beam, not with the individual particles. For the next generation of linear colliders, the beamstrahlung parameter happens to lie in the range between these two regimes. In this chapter, we shall describe these processes.

4.1 Coherent Pair Creation

4.1.1 Pair Creation in External Fields

A photon in vacuum is always accompanied with virtual electron-positron pairs (vacuum polarization). These pairs cannot emerge as real particles due to energy-momentum conservation. When in a strong electro-magnetic field, however, the energy-momentum can be carried by the field and the pair can be kicked ‘on-shell’. Consider the boosted frame where the e^+e^- pair is created at rest. In this frame there is an electric field which is $E' = (\hbar\omega/2mc^2)B$, where B is the magnetic field in the lab frame. At the threshold, the created particle with unit charge e should acquire enough energy within one Compton wavelength to supply for its rest mass. Thus the threshold condition is $eE'\lambda_e \sim mc^2$. Let us define a parameter χ as

$$\chi \equiv \frac{\omega}{m} \frac{B}{B_c} \equiv \frac{\omega}{E} \Upsilon \equiv y\Upsilon. \quad (4.74)$$

The last two definitions is convenient when the photon is induced by a primary particle with energy E in the lab frame. Thus $\chi \sim 1$ corresponds to the threshold condition for the coherent pair creation. It plays a similar role as Υ does in beamstrahlung.

The problem of pair creation in magnetic field is not new. Klepikov[24] first calculated this problem in uniform magnetic field. Several others[25] have re-examined the problem with different formalisms. In the lowest order approximation of the perturbation theory the matrix element for the pair creation process is essentially the same as that for

beamstrahlung, *c.f.* eq.(3.58), except that now the initial electron momentum k_μ has to be replaced by $-k_\mu$ in the cross channel.

The number spectrum as a function of energy of pair creation per unit time can then be obtained directly from eq.(3.58):

$$\frac{dW_{CP}}{dE_+} = \frac{\alpha}{\sqrt{3\pi}} \frac{m^2}{\omega^2} F_{CP} \quad (4.75)$$

with

$$F_{CP} = \int_{\eta}^{\infty} K_{1/3}(\eta') d\eta' + \left(\frac{E_-}{E_+} + \frac{E_+}{E_-} \right) K_{2/3}(\eta), \quad \eta = \frac{2}{3\chi} \frac{\omega^2}{E_+ E_-}, \quad E_- = \omega - E_+ \quad (4.76)$$

where E_{\pm} is the energy of the created e^{\pm} .

The total probability of pair creation per unit time is obtained by integrating this expression over ω . We find

$$W_{CP} = \int_0^{\omega} \frac{dW_{CP}}{dE_+} dE_+ = \begin{cases} 0.23(\alpha m^2/\omega) \chi e^{-8/3\chi} & (\chi \ll 1) \\ 0.38(\alpha m^2/\omega) \chi^{2/3} & (\chi \gg 1) \end{cases} \quad (4.77)$$

We see that $\chi \sim 1$ indeed corresponds to a threshold below which the probability is exponentially small. For the entire range of χ , W_{CP} can be well approximated by the following expression:[26]

$$W_{CP} \approx \frac{4}{25} \frac{\alpha m^2}{\omega} K_{1/3}^2\left(\frac{4}{3\chi}\right), \quad (4.78)$$

or simply by

$$W_{CP} \approx \frac{\alpha m^2}{\omega} \frac{0.23\chi}{(1 + 0.22\chi)^{1/3}} e^{-8/3\chi}, \quad (4.79)$$

where the coefficients are chosen so as to satisfy eq.(4.77).

The energy spectrum (4.76) (normalized to unity) is plotted in Fig.13 for various values of χ . We find that, when χ is small, the spectrum has a peak at $E_+/\omega=0.5$, which means the final electron and positron equally share the energy of the initial photon. On the other hand when $\chi \gg 1$, the maximum is around $E_{\pm}/\omega \sim 1.6/\chi$.

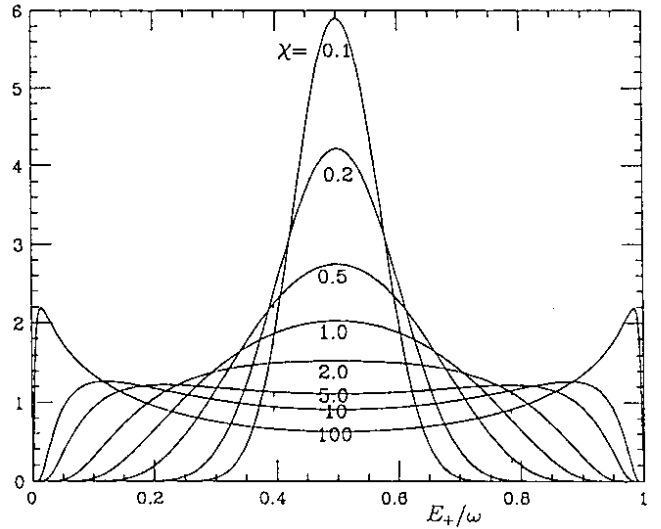
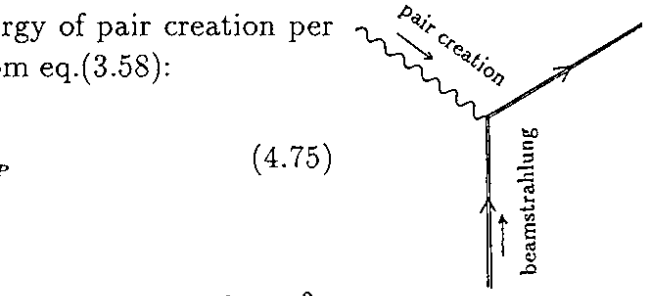


Fig.13. Energy distribution of e^+ from coherent pair creation for various values of χ .

4.1.2 Coherent Beamstrahlung Pair Creation

The beamstrahlung is the most important source of photons as the initial photon for the coherent pair creation process in linear colliders. For this purpose, it is useful to

express the energy spectrum (4.76) in terms of Υ of the primary particle instead of χ of the intermediate photon. Let $x \equiv E_+/E$ be the fractional energy of the pair particle and $y \equiv \omega/E$ be that of the photon, then $(E_+/\omega)\chi = x\Upsilon$. Then, eq.(4.76) becomes $dW_{CP}/dx = (\alpha m/\sqrt{3}\pi\gamma y^2)F_{CP}$ with

$$F_{CP}(x, y, \Upsilon) = \int_{\eta}^{\infty} K_{1/3}(\eta') d\eta' + \left(\frac{y-x}{x} + \frac{x}{y-x} \right) K_{2/3}(\eta), \quad \eta = \frac{2}{3\Upsilon} \frac{y}{x(y-x)}. \quad (4.80)$$

Then, the energy spectrum of the created particle through the cascade process of beamstrahlung and coherent pair creation is obtained by the convolution of eq.(3.59) and eq.(4.80) as

$$\begin{aligned} \frac{dn_b}{dx} &= \iint_{t_2 > t_1} dt_2 dt_1 d\omega \frac{dW_{\gamma}}{d\omega} \frac{dW_{CP}}{dx} \\ &= \frac{1}{3\pi^2} \left(\frac{\alpha}{\gamma\lambda_e} \right)^2 \iint dt_2 dt_1 \int_x^1 \frac{dy}{y^2} F_{BS}(y, \Upsilon(t_1)) F_{CP}(x, y, \Upsilon(t_2)). \end{aligned} \quad (4.81)$$

Here, t_1 and t_2 are the time of photon emission and pair creation, respectively. In the case of longitudinally uniform beams with small disruption, Υ is almost a constant along the photon path and we can replace $\iint dt_1 dt_2$ with $3\sigma_z^2/2$. Then the total number of pairs per primary electron is given by integrating this expression over x ;

$$n_b = \frac{3\sigma_z^2}{2} \int dy \frac{dW_{\gamma}}{dy} W_{CP} = \left[\frac{\alpha\sigma_z}{\gamma\lambda_e} \Upsilon \right]^2 \Xi(\Upsilon). \quad (4.82)$$

(This definition of Ξ is different from that in[31] by a numerical factor.) The function Ξ is plotted in Fig.14. Its asymptotic form is

$$\Xi(\Upsilon) = \begin{cases} (7/128) \exp(-16/3\Upsilon), & (\Upsilon \lesssim 1); \\ 0.295\Upsilon^{-2/3}(\log \Upsilon - 2.488), & (\Upsilon \gg 1). \end{cases} \quad (4.83)$$

As we have pointed out in Sec.3, the quantity $\alpha\sigma_z\Upsilon/\gamma\lambda_e$ is order unity for next generation colliders. Thus $n_b \sim O(10^{-2})$ for $\Upsilon \gtrsim 1$. Since the typical number of particles in a bunch is $\sim O(10^{10})$, we expect to have $\sim O(10^8)$ e^+e^- pairs per collision. On the other hand, Ξ is exponentially small for $\Upsilon \ll 1$. If we are to suppress the coherent creation below ~ 1 per collision we need to choose $\Upsilon \lesssim 0.3$ which gives $\Xi \lesssim 10^{-9}$. (In this context, it is better to use Υ_{max} instead of Υ_{avr} .)

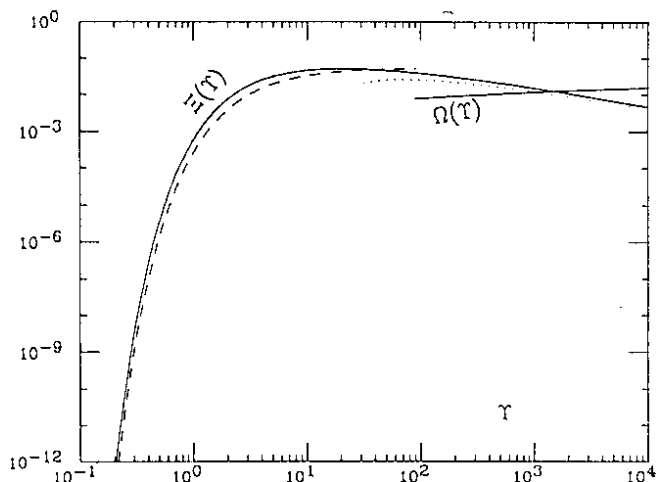


Fig.14. The functions $\Xi(\Upsilon)$ and $\Omega(\Upsilon)$. The dashed and the dotted lines are the asymptotic forms (4.83).

Next, let us discuss the energy spectrum. As seen in Fig.13 low energy pairs are strongly suppressed in coherent pair creation. To see this in more detail we plotted $dW_{CP}/d(\Upsilon x)$ as a function of $x\Upsilon$ in Fig.15 for various combinations of Υ and the intermediate photon energy y . One finds that, for a given value of Υ , the minimum energy x_{min} is independent of the intermediate photon energy. In addition, for different values of Υ 's, x_{min} scales as $1/\Upsilon$. This can be explained by the following qualitative arguments:

In the Lorentz frame where the pair is created at rest, the invariant mass of the system is $W = 2eE'\lambda_e$. The Lorentz factor for the boost is obviously the photon energy ω divided by the invariant mass. Thus we have $W^2 = 2eB\omega\lambda_e$. On the other hand, from the final state we have $W^2 = \omega^2 m^2/E_+E_-$. In the case where one particle is at very low energy, e.g., $E_+ \ll E_- \sim \omega$, we have $W^2 \sim \omega m^2/E_+$. Thus $E_{min} \sim \gamma m/2\Upsilon$, or $x_{min} \sim 1/2\Upsilon$, and is independent of the photon energy. The actual value of x_{min} is somewhat different from this naive picture, depending on how small a fraction one allows. One can take $x_{min} \sim 1/20\Upsilon$ if the conversion rate from a photon to a pair is to be less than $\sim 10^{-8}$.

The entire spectrum from the coherent beamstrahlung pair creation is plotted in Fig.16 (normalized to unity). As was pointed out in [28], the maximum is near $x=1/3$ when Υ is small. The peak moves towards small x for large Υ . If Υ is not very large ($\Upsilon \lesssim 10$), the following formula gives a good approximation for any x :

$$\frac{dn_b}{dx} = \left[\frac{\alpha \sigma_z}{\gamma \lambda_e} \Upsilon \right]^2 0.2 \sqrt{\frac{1-x}{\Upsilon x}} \times \exp \left[-\frac{2}{3\Upsilon} \left(\frac{1-x}{x} + \frac{4}{1-x} \right) \right] \quad (4.84)$$

The beamstrahlung photon is definitely polarized in the orbital plane of the electron. It was pointed out by Baier *et al.*[28] that the polarization effect can be taken into account in eq.(4.81) by replacing $F_{BS}F_{CP}$ with $F_{BS}F_{CP} - K_{2/3}(\xi)K_{2/3}(\eta)$ where ξ and η are defined in eqs.(3.60) and (4.80). Then, the factor $7/128$ in eq.(4.83) becomes $3/64$. There is no

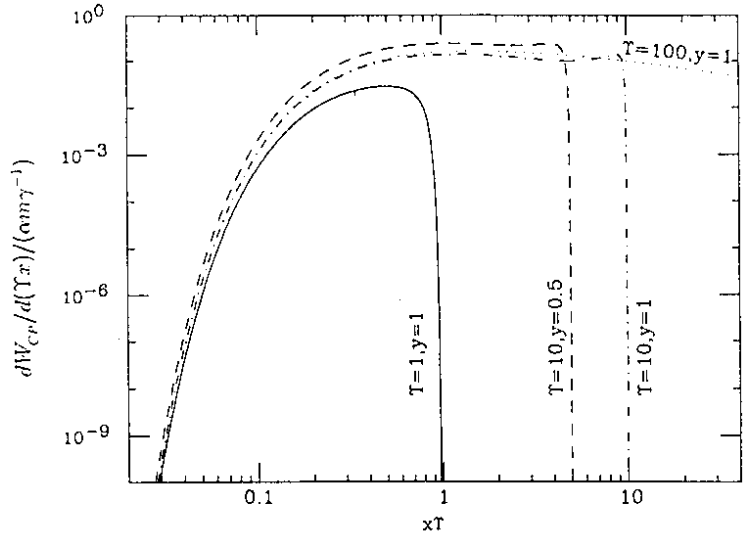


Fig.15. $dW_{CP}/d(\Upsilon x)/(\alpha m \gamma^{-1})$ vs. $x\Upsilon$.

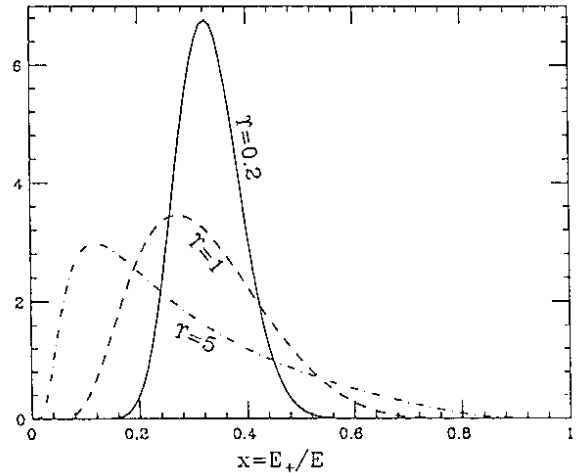


Fig.16. Energy spectrum of the cascade of beamstrahlung and coherent pair creation.

considerable effect on the spectrum.

4.1.3 The Trident Cascade

In addition to the coherent beamstrahlung pair creation, e^+e^- pairs can also be coherently created through virtual photons carried by the primary charged particles, i.e., $e \rightarrow ee^+e^-$, in an electro-magnetic field. This process is sometimes called the *trident cascade*, for an obvious reason. It has been previously studied in details[29]. For the sake of comparison, we express it as

$$n_v = \left(\frac{\alpha\sigma_z}{\gamma\lambda_e} \Upsilon \right) \Omega(\Upsilon), \quad (4.85)$$

where, according to Ritus[30],

$$\Omega(\Upsilon) \sim 0.23 \alpha \log \Upsilon, \quad \Upsilon \gg 1. \quad (4.86)$$

The auxiliary function $\Omega(\Upsilon)$ is also shown in Fig.14. In addition to the different scalings between Ξ and Ω , the beamstrahlung pair creation increases quadratically with the quantity $(\alpha\sigma_z/\gamma\lambda_e)\Upsilon$, while the trident cascade scales linearly. This is simply because the former necessarily involves a real intermediate process and thus a double integration in time. Notice that the cross-over between $\Xi(\Upsilon)$ and $\Omega(\Upsilon)$ occurs at $\Upsilon \sim 1000$. Since the quantity $(\alpha\sigma_z/\gamma\lambda_e)\Upsilon$ is usually of the order unity, we see that the contribution from the trident cascade is relatively unimportant unless $\Upsilon \gg 1$.

4.1.4 Deflection Angle and Maximum Υ

If the e^+e^- pair is created in a field-free space, their outgoing angles will be simply the final angles from the creation process. In the case of beam-beam interaction, however, these low energy secondary particles will be strongly deflected by the macroscopic collective field. The deflection angle of low energy particle is discussed in Sec.2.5.

If a e^+e^- collider is designed such that the beams are colliding head-on, then the above consideration imposes a severe constraint on its design. The typical distance between the final focusing magnet and the IP is $\sim 10^2$ cm, while the aperture of the magnet is $\sim 10^{-1}$ cm. This means that any particle with outgoing angle larger than $\sim O(1)$ millirad will necessarily hit the magnet and generate backgrounds.

One obvious way to alleviate the problem is to sufficiently suppress the coherent process. This can in principle be achieved by imposing a constraint on the value of Υ . As we have seen, if $\Upsilon \lesssim 0.3$, the pair creation rates are exponentially suppressed to $\sim O(10^{-9})$. To achieve this goal, one needs to reduce the charge density of the beams by either lengthening the bunch or reducing the number of particles per bunch, or both, with a corresponding increase in the number of bunches in order not to sacrifice the luminosity. In practice, however, these leverages can be handled only within certain limits due to various other accelerator constraints.

It happens that it is not necessary to entirely suppress the coherent pairs[31]. Remember that for any given Υ there is a minimum x_{min} . Assume that the beams are colliding

at an angle ϕ_c . Then by inserting x_{min} into eq.(2.43), one finds the maximum allowable value of Υ to suppress almost perfectly the large angle pairs $\theta \gtrsim \phi_c$:

$$\Upsilon \lesssim \max \left(0.3, \frac{\sqrt{3}}{20} \frac{(\phi_c \sigma_z / \sigma_x)^2}{\log[5(\phi_c \sigma_z / \sigma_x)^2]} \right). \quad (4.87)$$

(The factor 5 in the log is somewhat arbitrary.) When the crossing angle is much larger than the beam diagonal angle σ_x / σ_z , this limit is much less stringent than the constraint for total suppression of the coherent pairs.

4.2 Incoherent Pair Creation

The seriousness of the pair creation problem lies in the transverse momenta that the pair particles carry when leaving the interaction point (IP) with large angles. In the next generation of linear colliders, as it occurs, the coherent pairs can be exponentially suppressed by properly choosing the Υ ($\lesssim 0.3$). When this is achieved, the incoherent pair creation processes, where the e^+e^- pairs are created through individual scatterings, becomes dominant. Furthermore, these incoherent pairs tend to have more uniform energy spectra than the coherent process, resulting in relatively more abundance of deleterious low energy particles.

Notice that both real (beamstrahlung) and virtual photons can turn into e^+e^- pairs through this channel. These are the so-called Breit-Wheeler ($\gamma\gamma \rightarrow e^+e^-$), Bethe-Heitler ($e^\pm\gamma \rightarrow e^\pm e^+e^-$) and Landau-Lifshitz ($e^+e^- \rightarrow e^+e^-e^+e^-$) processes. In this section, we will describe the spectrum, the cross section, and the large inherent angle events of the incoherent pair creation processes using the *equivalent photon approximation*. Numerical examples are given wherever suitable.

4.2.1 The Equivalent Photon Approximation

The Breit-Wheeler, Bethe-Heitler, and Landau-Lifshitz processes are well-known phenomena in QED, and are well described in any standard QED textbook[32]. In our particular setting, the BW and BH processes occur as a result of beamstrahlung, which has a wide range of spectrum. Thus for our purpose it is most convenient to describe these processes in the laboratory (lab) frame (which is also the center-of-mass frame for the colliding e^+e^- beams.) Moreover, we notice that the basic kernel of all these processes is the same. For the BW process both photons are real beamstrahlung photons; for the BH process one is real and one is virtual; and for the LL process both photons are virtual.

We shall thus invoke the so-called equivalent photon picture in our discussion. This is an approximation in which the two photons involved in each process are treated to be real. Then the relativistic kinematics relates the fractional energy x of the outgoing positron (or electron) to its angle θ (relative to the initial particle trajectory) and the fractional energies of the two photons, y_1, y_2 , as

$$x = \frac{2y_1y_2}{y_1(1 - \beta c) + y_2(1 + \beta c)}, \quad (4.88)$$

where $c \equiv \cos \theta$ and β is the speed of the particle. In the following, we shall assume $\beta \sim 1$, as the pair particles of concern are still relativistic.

The differential cross section for the kernel $\gamma\gamma \rightarrow e^+e^-$ is

$$d\alpha_{\gamma\gamma} = \frac{8\pi r_e^2 m^2 dt}{s^2} \left[\frac{1}{4} \left(\frac{t-m^2}{u-m^2} + \frac{u-m^2}{t-m^2} \right) - \left(\frac{m^2}{t-m^2} + \frac{m^2}{u-m^2} \right) - \left(\frac{m^2}{t-m^2} + \frac{m^2}{u-m^2} \right)^2 \right], \quad (4.89)$$

where s, t, u are the Mandelstam variables. In terms of our variables, we have

$$s = 4\gamma^2 m^2 y_1 y_2, \quad t - m^2 = -2\gamma^2 m^2 y_1 x(1-c), \quad u - m^2 = -2\gamma^2 m^2 y_2 x(1+c). \quad (4.90)$$

With the help of eq.(4.88), we find

$$d\alpha_{\gamma\gamma} = \frac{\pi}{4} \frac{r_e^2}{\gamma^2 y_1 y_2} \frac{dc}{y_2} \left\{ 2 \frac{y_1^2(1-c)^2 + y_2^2(1+c)^2}{(1-c^2)[y_1(1-c) + y_2(1+c)]} + \frac{2}{\gamma^2} \frac{y_1(1-c) + y_2(1+c)}{y_1 y_2 (1-c^2)} - \frac{1}{2\gamma^4} \frac{[y_1(1-c) + y_2(1+c)]^3}{y_1 y_2 [y_1 y_2 (1-c^2)]^2} \right\}. \quad (4.91)$$

The first term obviously dominates. Furthermore, we expect that the major contribution comes from $c \lesssim c_0 \lesssim 1$. Thus, $y_1(1-c) + y_2(1+c) \sim 2y_2$. With $\gamma^2 y_1 y_2 \gg 1$, we arrive at

$$\alpha_{\gamma\gamma}(y_1, y_2) = \frac{d\alpha_{\gamma\gamma}}{dc} \sim \frac{\pi r_e^2}{\gamma^2 y_1 y_2} \frac{1}{1-c^2} \left\{ \frac{y_1^2(1-c)^2 + y_2^2(1+c)^2}{[y_1(1-c) + y_2(1+c)]^2} \right\} \sim \frac{\pi r_e^2}{\gamma^2 y_1 y_2} \frac{1}{1-c^2}. \quad (4.92)$$

The last approximation is made due to the fact that the factor in the parenthesis is a slow varying function ranging from 1/2 to 1. In so doing our estimates are upper bounds which is too big by less than a factor of 2.

Next we need to find the spectrum for the virtual photons that comove with the primary charged particle. From the virtual photon propagator, one can establish the spectrum of the equivalent photons;

$$dn_\nu = \frac{\alpha}{\pi} \frac{dy}{y} \frac{y_\perp^2 dy_\perp^2}{(y_\perp^2 + y^2/\gamma^2)^2}, \quad (4.93)$$

where y_\perp is the normalized transverse momentum q of the photon: $y_\perp \equiv q/\gamma m$. Integrating over y_\perp^2 , we get

$$n_\nu(y) = \frac{\alpha}{\pi} \frac{1}{y} \log \left(\frac{y_{\perp max}^2 + y^2/\gamma^2}{y_{\perp min}^2 + y^2/\gamma^2} \right), \quad (4.94)$$

where $y_{\perp max}$ and $y_{\perp min}$ are the maximum and minimum momentum transfer, respectively. In the equivalent photon approximation, it is assumed that the transverse momentum of the virtual photon satisfies the condition

$$y/\gamma^2 \ll y_\perp \ll 1/\gamma. \quad (4.95)$$

Since n_ν depends on $y_{\perp max}$ and $y_{\perp min}$ only logarithmically, it is customary to take the bounds in eq.(4.95) as their values. We then have

$$n_\nu(y) = \frac{2\alpha}{y} \frac{1}{y} \log \left(\frac{1}{y} \right). \quad (4.96)$$

This expression is indeterminate up to a numerical coefficient in the argument of the logarithm due to the nature of the approximation[22]. In the equivalent photon approximation, one combines this virtual photon spectrum with the above differential cross section to obtain the desired expression for the process of which involves a virtual photon exchange.

4.2.2 The Total Cross Sections

We now want to find the total incoherent e^+e^- pair creation events:

$$\sigma = g \int dc \int dy_2 \int dy_1 n_a(y_1) n_b(y_2) \alpha_{\gamma\gamma}(y_1, y_2), \quad (4.97)$$

where $g=1/4$ for the BW process and 1 for both BH and LL processes, respectively. For the BW process, the effective collision time for the beamstrahlung photons, which are emitted during the collision itself, is only 1/4 of that of the primary beam particles. For the BH process, the factor 1/2 that arises from the effective collision time is compensated by the matching between the real and the virtual photons from both beams. The photon spectra n_a and n_b depend on whether the photons are real or virtual. For virtual photons, it is the spectrum derived in Sec.4.2.1. For real beamstrahlung photons, the spectrum is given in (3.58). For our purpose here, we integrate it over the collision time and approximate it in the form

$$n_b(y) = \frac{\Gamma(2/3)}{\pi} \left(\frac{\alpha\sigma_z}{\gamma\lambda_e} \right) (3\Upsilon)^{2/3} y^{-2/3}, \quad (4.98)$$

where $\Gamma(2/3)=1.3541$.

First we carry out the angular integration. The dominant contribution to the cross section is associated with the typical transverse momentum m versus half of the center-of-mass energy $\sqrt{\omega_1\omega_2} = m\gamma\sqrt{y_1y_2}$, or $\theta_0 \sim 1/\gamma\sqrt{y_1y_2}$. Thus for the BW process with fixed initial photon energies in the lab frame, we have

$$\sigma_{BW}(y_1, y_2) = \int_{-c_0}^{c_0} \alpha_{\gamma\gamma}(y_1, y_2) dc = \frac{\pi r_e^2}{2\gamma^2 y_1 y_2} \log(4\gamma^2 y_1 y_2). \quad (4.99)$$

For the BH and LL processes we need to further integrate over the virtual photon spectrum. The threshold condition for pair creation is that $m = \sqrt{\omega_1\omega_2}$. Thus the lower bound for the virtual photon energy with a fixed real photon energy y_1 is $y_2 = 1/(\gamma^2 y_1)$. We then have, for the BH process,

$$\sigma_{BH}(y_1) = \int_{1/\gamma^2 y_1}^1 n_v(y_2) \sigma_{BW}(y_1, y_2) dy_2 = \alpha r_e^2 \{(\log 4 + 1) \log 4\gamma^2 y_1 - (\log 4 + 2) \log 4 - 1\}. \quad (4.100)$$

For the LL process, we need to integrate once more over the other virtual photon. Again from the threshold condition, the lower bound for the second photon is $1/\gamma^2$. Thus

$$\sigma_{LL} = \int_{1/\gamma^2}^1 dy_1 \int_{1/\gamma^2 y_1}^1 dy_2 n_v(y_1) n_v(y_2) \sigma_{BW}(y_1, y_2) = \frac{\alpha r_e^2}{\pi} (\log 4 + 1) \left(\frac{1}{3} \log^3 \gamma^2 - 2 \log^2 \gamma^2 \right). \quad (4.101)$$

When compared with the more accurate calculations[32,33]

$$\sigma_{BH}(y_1) = (28/9)\alpha r_e^2 \log(4\gamma^2 y_1) \quad (4.102)$$

$$\sigma_{LL} = (\alpha^2 r_e^2 / \pi) [(28/27) \log^3(4\gamma^2) - 6.59 \log^2(4\gamma^2) - 11.8 \log(4\gamma^2) + 104], \quad (4.103)$$

we find that σ_{BW} has the precise logarithmic term and, while both σ_{BH} and σ_{LL} indeed reproduce the correct logarithmic behavior, our expressions tend to have somewhat smaller coefficients. This, however, is consistent with the accuracy of our approximations.

The above intermediate expressions serve to compare with the well-known QED results. In our specific context, the real photons are induced from beamstrahlung. Thus for the BW and BH processes we further combine with beamstrahlung spectrum, with the proper g factor in (4.97) included, and get

$$\sigma_{BW} = \frac{3}{16\pi} \Gamma^2(2/3) \frac{r_e^2}{\gamma^{2/3}} \left(\frac{\alpha \sigma_z}{\gamma \lambda_e} \right)^2 (3\Upsilon)^{4/3} \left[\log 4 + \frac{3}{2} \right] \log \gamma^2, \quad (4.104)$$

$$\sigma_{BH} = \frac{3}{\pi} \Gamma(2/3) \alpha r_e^2 \left(\frac{\alpha \sigma_z}{\gamma \lambda_e} \right) (3\Upsilon)^{2/3} [(\log 4 + 1) \log 4\gamma^2 - (\log 4 + 5) \log 4 - 4]. \quad (4.105)$$

Consider a 1/2 TeV Intermediate Linear Collider (ILC) designed by Palmer[35] (Palmer's Machine I), where $\gamma = 5 \times 10^5$, $\sigma_z = 0.11\text{mm}$, $\Upsilon = 0.17$ and luminosity $L = 1.95 \times 10^{31}/\text{cm}^2/\text{bunch train}$ (10 bunches per train) and 130Hz collision repetition rate. The total cross sections in (4.101)-(4.105) are

$$\sigma_{BW} \approx 8 \times 10^{-28} \text{cm}^2 \quad ; \quad \sigma_{BH} \approx 1 \times 10^{-25} \text{cm}^2 \quad ; \quad \sigma_{LL} \approx 2 \times 10^{-28} \text{cm}^2. \quad (4.106)$$

The total number of pairs are then $N_{BW} \approx 2 \times 10^4$, $N_{BH} \approx 2 \times 10^6$ and $N_{LL} \approx 3 \times 10^5$, per bunch train.

For a 1 TeV linear collider (TLC) (Palmer's Machine J), where $\gamma = 1 \times 10^6$, $\sigma_z = 0.12\text{mm}$, $\Upsilon = 0.60$, one finds that the cross sections are essentially the same. With a luminosity $L = 8.04 \times 10^{31}/\text{cm}^2/\text{bunch train}$ (17 bunches per train), the incoherent pairs are about 4 times more than that of ILC. These are about two to three orders of magnitude smaller than the corresponding coherent yields.

4.2.3 Pair Creation at Large Inherent Angles

Since the central issue is the transverse momentum for particles with large angles, we notice that there is another source for it, in addition to the deflections due to the collective fields of the oncoming beam. Namely, when the pair particles are created at low energies, the intrinsic angles of these pairs when produced may already be large. This issue was first studied by Zolotarev et al.[22], and more recently by Chen et al.[34]

To obtain the partial cross sections for all events with transverse momentum (divided by γm) $p_\perp \geq p_{\perp 0}$ and outgoing angle $\theta_0 \leq \theta \leq \pi - \theta_0$ (or $-c_0 \leq c \leq c_0$), it is more convenient to first carry out the integrations over y_1 and y_2 in (4.97). Since the transverse momentum $p_\perp = x\sqrt{1-c^2}$, with any choice of p_\perp and c , the initial photon energies are limited by

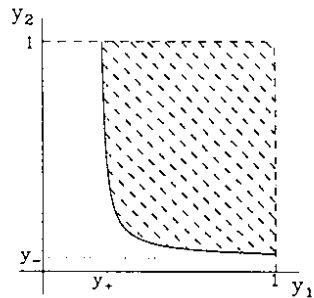
$$y_\pm = \frac{x}{2}(1 \pm c) = \frac{p_\perp}{2} \sqrt{\frac{1 \pm c}{1 \mp c}}. \quad (4.107)$$

Furthermore, for any given value of $y_2 \geq y_1$, the lower bound for y_1 is

$$y_b = \frac{y_2 y_+}{y_2 - y_-}. \quad (4.108)$$

Equation (4.97) can then be specified as

$$\sigma_{ab \rightarrow e^+}(p_{\perp 0}, c_0) = g \int_{-c_0}^{\infty} dc \int_{y_-}^{\infty} dy_2 \int_{y_b}^{\infty} dy_1 n_a(y_1) n_b(y_2) \alpha_{\gamma}(y_1, y_2). \quad (4.109)$$



The upper limits of the spectral integrals are set at infinity since the contributions are essentially dominated by the lower bounds.

Inserting the photon spectra and eq.(4.92) into eq.(4.109) and invoking the boundary conditions in eqs.(4.107) and (4.108), we can calculate the partial cross section for positrons with momentum larger than $p_{\perp 0}$ in all 4π solid angle, excluding the forward and backward cones of half-angle θ_0 . The results are[34]

$$\sigma_{BW} = \frac{9}{8\pi} \frac{\Gamma^4(2/3)}{\Gamma(1/3)} \frac{r_e^2}{\gamma^2} \left[\frac{\alpha \sigma_z}{\gamma \lambda_e} \right]^2 \left[\frac{6\Upsilon}{p_{\perp 0}} \right]^{4/3} \log \frac{1}{\tau_0}; \quad (4.110)$$

$$\sigma_{BH} = \frac{54}{5\pi} \Gamma\left(\frac{2}{3}\right) \frac{\alpha r_e^2}{\gamma^2} \frac{\alpha \sigma_z}{\gamma \lambda_e} \left[\frac{36\Upsilon^2}{p_{\perp 0}^5} \right]^{1/3} [\tau_0^{-1/3} - \tau_0^{1/3}] \left[-\log \frac{p_{\perp 0} \tau_0}{2} - \psi\left(\frac{8}{3}\right) + \psi(1) \right]; \quad (4.111)$$

$$\sigma_{LL} = \frac{16}{\pi} \frac{\alpha^2 r_e^2}{\gamma^2} \frac{1}{p_{\perp 0}^2} \log \frac{1}{\tau_0} \left[\log \frac{p_{\perp 0}}{2\tau_0} \log \frac{p_{\perp 0} \tau_0}{2} + 3 \log(p_{\perp 0}/2) + \frac{73}{12} - \frac{\pi^2}{6} \right]. \quad (4.112)$$

Here $\Gamma(1/3)=2.6789$, $\psi(8/3)=0.7818$, $\psi(1)=0.5772$ and $\tau_0 = \tan(\theta_0/2)$. We note that both BW and LL processes are forward-backward symmetric, while BH is asymmetric in c . This is the result of the matching between the two different photon spectra in the BH case.

The above expressions account for only one of the two particles (say positron) in the e^+e^- pairs. In the case where the inherent transverse momentum and angle are already large, further deflections on either species in the pair by the beam should not effectively alter the ultimate outgoing transverse momenta and angles. Therefore both electrons and positrons, irrespective of the directions of flight, should be counted. So the contribution should be twice of what would be given from the partial cross sections in eqs.(4.110)-(4.112).

Let us again estimate the yields from ILC and TLC. First we plot the partial cross sections in eqs.(4.110)-(4.112) and their sum as a function of $p_{\perp 0}$ in Fig.17, with the cut-off angle fixed at $\theta_0=0.1$. The dominant scalings of $p_{\perp 0}^{-4/3}$, $p_{\perp 0}^{-5/3}$ and $p_{\perp 0}^{-2}$, for the BW, BH and LL processes, respectively, are clearly seen. On the other hand, the dependence of the partial cross sections on the cut-off angles is much milder, as expected. Fig.18 shows such a plot, again with the ILC parameters and $p_{\perp 0}=10\text{MeV}/c$. The choice of the cut-offs depends on the practical considerations in the design of the detector masking[36]. From Ref.[31] it should be reasonable to assume $\theta_0=100\text{mrad}=0.1$ and the transverse momentum cut-off at $10\text{MeV}/c$, or $p_{\perp 0}=4 \times 10^{-5}$. The total number of large inherent angle e^+ and e^- is obtained simply by doubling the partial cross sections in eqs.(4.110)-(4.112) and multiplying by the luminosity. The corresponding events per bunch train are $N_{BW} \approx 220$, $N_{BH} \approx 1230$ and $N_{LL} \approx 500$. So the total yield per bunch is $\approx 2 \times 10^3$.

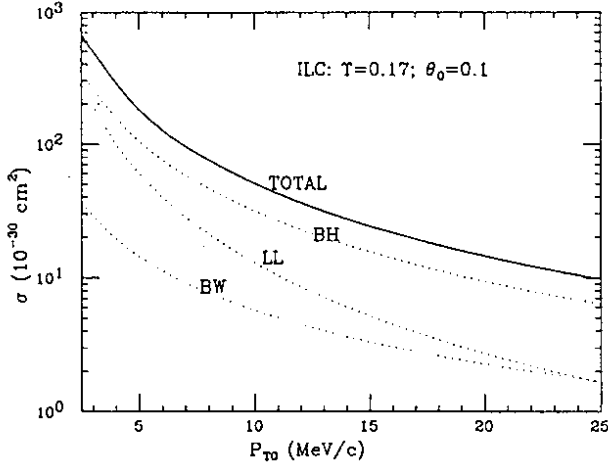


Fig.17. The partial cross section as a function of the cut-off transverse momentum, at a fixed cut-off angle $\theta_0=0.1$, for the BW, BH and LL processes, shown in dotted curves. The sum of these three processes is shown in solid curve. The parameters are based on the ILC in Ref.[35].

For TLC, we find, for every bunch train $N_{BW} \approx 900$, $N_{BH} \approx 5300$ and $N_{LL} \approx 2400$. The total yield is $\approx 9 \times 10^3$. These numbers are not small.

In order to further suppress the yield, it is most effective to increase the longitudinal solenoidal magnetic field in the detector so as to raise the cut-off transverse momentum. The dependence of the total events on the transverse momentum cut-off for the ILC and TLC is shown in Fig.19, where the angular cut-off is fixed at $\theta_0=0.1$.

4.2.4 Geometric Reduction

In Sec. 4.2.2 and 4.2.3 we see that for a given equivalent photon energy y_1 , the dominant contribution to the cross section comes from the region of small transverse momentum y_{bot} . Quantum mechanically, this corresponds to the region of large *impact parameters*: $b \sim 1/q_{\perp} = 1/(\gamma m y_{\perp})$, upto a typical value of $b_m \sim 1/m y = \lambda_e/y$. If b_m turns out to be larger than the beam transverse size, these equivalent photons would extend physically to the outside of the oncoming beam. As a result, the part of the equivalent photons that have impact parameters larger than the beam size cannot participate in the interaction. Therefore the effective cross section will be smaller than the standard calculations.

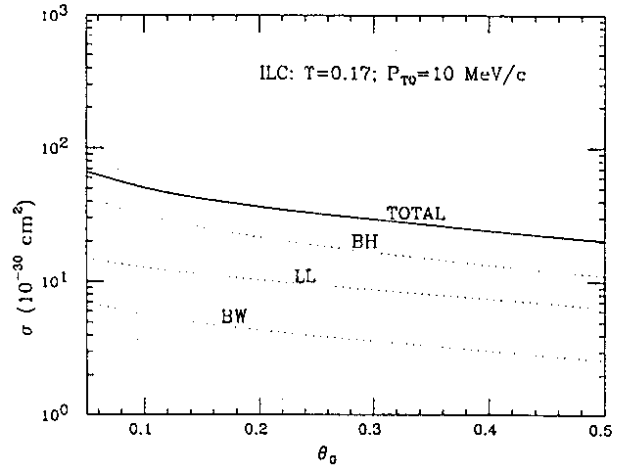


Fig.18. The partial cross section as a function of the cut-off angle. The transverse momentum cut-off is fixed at $p_{\perp 0}=10\text{MeV}/c$. The same ILC parameters are assumed.

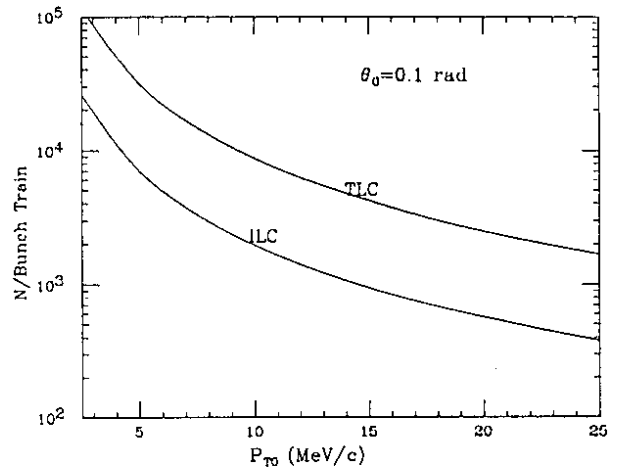


Fig.19. The total yield of pair particles in ILC and TLC per bunch train as a function of the transverse momentum cut-off.

This *geometric reduction* effect was first observed at Novosibirsk[37,38], and subsequently developed theoretically by several authors[39,40,21].

For the next generation linear colliders, such as ILC and TLC that we discussed above, the e^+e^- colliding beams are typically very *flat*, i.e., $\sigma_x \gg \sigma_y$. Thus the geometric reduction is dominated by the minor dimension. Let the typical beam height be $2\sigma_y$, then the corresponding “cut-off” impact parameter is $b_c \sim 2\sigma_y$. Thus the region of transverse momentum transfer: $1/b_c \gtrsim q_\perp \gtrsim 1/b_m$ is suppressed. Let us denote the effective cross section by $\bar{\sigma} = \sigma - \sigma'$, then the cut-off cross section σ' is associated with the equivalent photon spectrum in (4.94) where $y_{\perp max}$ and $y_{\perp min}$ are related to b_m and b_c , respectively, i.e.,

$$n'_\nu(y) \simeq \frac{2\alpha}{\pi} \frac{dy}{y} \log\left(\frac{\lambda_e/2\sigma_y}{y}\right). \quad (4.113)$$

The cut-off cross section σ' for the BH and LL processes can be derived by inserting n'_ν into (4.100) and (4.101). By construction, the above spectrum is applicable for $y \lesssim \lambda_e/2\sigma_y$. Thus the upper bound of the y -integrations have to be replaced by $\lambda_e/2\sigma_y$. But since the dominant contribution comes from the lower bounds, this change does not affect the leading logarithmic behavior. We find the reduced effective cross section to be

$$\bar{\sigma}_{BH} \sim \alpha r_e^2 (\log 4 + 1) \log(2\sigma_y/\lambda_e), \quad (4.114)$$

$$\bar{\sigma}_{LL} \sim \frac{1}{3\pi} \alpha^2 r_e^2 (\log 4 + 1) [\log^3 \gamma^2 - \log^3(\gamma^2 \lambda_e/2\sigma_y)]. \quad (4.115)$$

For ILC, the beam height is as miniscule as $2\sigma_y=8\text{nm}$. The geometric reduction turns out to be $\bar{\sigma}_{BH}/\sigma_{BH} \sim 0.36$ and $\bar{\sigma}_{LL}/\sigma_{LL} \sim 0.79$. For TLC, $2\sigma_y=6.2\text{nm}$. The corresponding reductions are 0.33 and 0.73 for the BH and LL processes, respectively. One could in principle also repeat the calculations of large inherent angles for the geometric reductions. As a rough estimate, the corresponding reductions should not be too different from the above values. The geometric reduction is therefore a welcoming effect concerning the e^+e^- backgrounds.

References

- [1] R. Holebeek, Nucl. Instr. Meth. 184 (1981) 333.
- [2] N. Solyak, *Flat Beam Disruption*, ICFA workshop on linear colliders, Capri, Italy, Jun.1988.
- [3] W. M. Fawley and E. P. Lee, *Particle in Cell Simulations of Disruption*, in ‘New Developments in Particle Acceleration Techniques’, Orsay 1987, CERN 87-11, ECFA 87/110.
- [4] P. Chen and K. Yokoya, *Disruption Effects from the Interaction of Round e^+e^- Beams*, Phys. Rev. D38 (1988) 987; K. Yokoya, Proc. 1988 Linear Acc. Conf. Oct 3-7, 1988, Williamsburg, Virginia. (CEBAF-Report 89-001, Jun.1989), page 494.
- [5] L. Wood, private communication. Some results appear in O. Napoly and B. Zotter, Proc. 2nd European Accelerator Conf., Nice, Jun.1990, page 1408.

- [6] K. Yokoya, *A Computer Simulation Code for the Beam-Beam Interaction in Linear Colliders*, KEK-report 85-9, Oct.1985.
- [7] Y. H. Chin, *Stability of a Colliding Beam in a Linear Collider*, DESY 87-011, Jan.1987.
- [8] P. Chen and K. Yokoya, *Multibunch Crossing Instability*, SLAC-PUB-4653, Jun.1988.
- [9] A. A. Sokolov and I. M. Ternov, 'Radiation from Relativistic Electrons', American Institute of Physics, Translation Series, New York, 1986.
- [10] V. N. Baier and V. M. Katkov, *Sov. Phys. JETP*, **26**(1968)854, **28**(1969)807.
- [11] K. Yokoya and P. Chen, *Electron Energy Spectrum and Maximum Disruption Angle under Multi-Photon Beamstrahlung*, Proc. IEEE Part. Acc. Conf, Chicago, IL, March 1989. SLAC-PUB-4935, Mar.1989.
- [12] M. Jacob and T. T. Wu, *Phys. Lett*, **197B**(1987)253, *Nucl. Phys*, **B303**(1988)373 and 389.
P. Chen and K. Yokoya, *Phys. Rev. Lett*, **61**(1988)1101.
M. Bell and J. S. Bell, *Part. Acc.* **22**(1988)301.
V. N. Baier, V. M. Katkov and V. M. Strakhovenko, *Quantum Radiation Theory in Inhomogeneous External Field*, INP-preprint 88-168, Novosibirsk, 1988.
- [13] R. B. Palmer, Workshop on New Developments in Particle Accelerator Techniques, Orsay, France, Jun.1987, SLAC-PUB-4295, Apr.1987.
- [14] D. H. Whittum, A. M. Sessler, J. J. Stewart and S. S. Yu, *Plasma Suppression of Beamstrahlung*, LBL-25759, Jun.1989.
- [15] N. Solyak, *Collision Effects in Compensated Bunches of Linear Colliders*, preprint 88-44, INP Novosibirsk, 1988.
- [16] J. B. Rosenzweig, B. Autin and P. Chen, *Instability of Compensated Beam-Beam Collisions*, In 'Advanced Accelerator Concepts', ed. C. Joshi, AIP Conf. Proceedings **193**(1989).
- [17] V. Telnov and P. Chen, *Phys. Rev. Lett* **63**(1989)1796.
- [18] V. Telnov, *Nucl. Instr. Meth.* **A294**(1990)72.
- [19] V. E. Balakin and A. A. Michailichenko, *The Conversion System for Obtaining Highly Polarized Electrons and Positrons*, INP-Preprint, 79-85, Novosibirsk, 1979.
A. A. Michailichenko, Proc. of Workshop on "Physics of Linear Colliders", Capri, Jun.13-17,1988, page 391.
- [20] K. Yokoya and P. Chen, *Depolarization due to Beam-Beam Interaction in Electron-Positron Linear Colliders*, 8-th International Symposium on High Energy physics, Minneapolis, Minnesota, Sept.1988. SLAC-PUB-4692, Sept.1988.

- [21] G. L. Kotkin, S. I. Polityko and V. G. Serbo, *Sov. J. Nucl. Phys.*, **42**(1985)440.
- [22] M. S. Zolotarev, E. A. Kuraev and V. G. Serbo, *Inst. Yadernoi Fiziki Preprint* 81-63(1981); SLAC TRANS-227(1987).
- [23] P. Chen, *Intl. Workshop on the Next Generation Linear Colliders*, SLAC Report 335, 1989; SLAC-PUB-4822 (1988), appeared in *Proc. DPF Summer Study, SNOWMASS '88*, World Scientific (1989).
- [24] N. P. Klepikov, *Sov. Phys. JETP* **19**(1954)19.
- [25] V. N. Baier and V. M. Katkov, *Sov. Phys. JETP* **26**(1968)854; W. Y. Tsai and T. Erber, *Phys. Rev.* **D10**(1974)492.
- [26] T. Erber, *Rev. Mod. Phys.* **38**(1966)626.
- [27] V. N. Baier, V. M. Katkov and V. M. Strakhovenko, *Phys. Lett.* **B225**(1989)193.
- [28] V. N. Baier, V. M. Katkov and V. M. Strakhovenko, *Part. Acc.* **30**(1990)43.
- [29] V. N. Baier, V. M. Katkov and V. M. Strakhovenko, *Soviet J. Nucl. Phys.* **14**(1972)572.
- [30] V. I. Ritus, *Nucl. Phys.* **B44**(1972)236.
- [31] P. Chen, *Part. Acc.* **30**(1990)1013.
- [32] See, for example, V. B. Berestetskii, E. M. Lifshitz and L. P. Pitaevskii, *Relativistic Quantum Theory*, Part 1, Pergamon Press (1971).
- [33] V. N. Baier, V. S. Fadin, V. A. Khoze and E. A. Kuraev, *Phys. Reports* **78**(1981)293.
- [34] P. Chen, T. Tauchi and D. V. Schroeder, *Pair Creation at Large Inherent Angles*, SLAC-PUB-, 1991; to appear in *Snowmass Proceedings*, 1991.
- [35] R. B. Palmer, SLAC-PUB-5190 (1990); submitted to *Ann. Rev. Nucl. Part. Sci.*
- [36] T. Tauchi, et al., *Background Problem at Interaction Point for an e^+e^- Linear Collider*, submitted to IEEE conf.
- [37] A. E. Blinov, A. E. Bondar, Yu. I. Eidelman, et al., *Phys. Lett.* **113B**(1982)423.
- [38] Yu. A. Tikhonov, *Candidates's Dissertation*, *Inst. Nucl. Phys.*, Novosibirsk (1982).
- [39] V. N. Baier, V. M. Katkov and V. M. Strakhovenko, *Sov. J. Nucl. Phys.* **36**(1982)95.
- [40] A. I. Burov and Ya. S. Derbenev, *INP Preprint* 82-07, Novosibirsk (1982).